Glass transition and density fluctuations in the fragile glass former orthoterphenyl

G. Monaco,[1] D. Fioretto,[2] L. Comez,[2] and G. Ruocco[3]
[1]*European Synchrotron Radiation Facility, Boîte Postale 220, F-38042 Grenoble Cedex 9, France*
[2]*Università di Perugia and Istituto Nazionale di Fisica della Materia, I-06123, Perugia, Italy*
[3]*Università di L'Aquila and Istituto Nazionale di Fisica della Materia, I-67100, L'Aquila, Italy*
(Received 24 October 2000; revised manuscript received 12 February 2001; published 22 May 2001)

High-resolution Brillouin light scattering is used to measure the dynamic structure factor of the fragile glass former orthoterphenyl (OTP) in a wide temperature range around the glass transition region and up to the boiling point. The whole set of spectra is described in terms of a phenomenological generalized hydrodynamic model. In the supercooled phase, we show the contemporary existence of the structural process, whose main features come out to be consistent with the results obtained with other spectroscopies, and of a secondary, activated process, which occurs on the 10^{-11} s time scale and has a low activation energy ($E_a^f = 0.28$ kcal/mol). This latter process, which is also present in the glassy phase and seems to be insensitive to the glass transition, is attributed to the coupling between the density modes and intramolecular degrees of freedom. In the normal liquid phase, the two processes merge together, and the resulting characteristic time is no longer consistent with those derived with other spectroscopies. The analysis points to the conclusion that, for what concerns the long-wavelength density fluctuations in fragile glass formers such as OTP, the universal dynamical features related to the glass transition come out clearly only in the supercooled phase and at frequencies lower than $\approx 10^6$ Hz.

DOI: 10.1103/PhysRevE.63.061502 PACS number(s): 64.70.Pf, 78.35.+c, 61.20.Lc, 62.60.+v

I. INTRODUCTION

The study of the glass transition and the study of the atomic dynamics in liquids are topics that are nowadays strongly connected. The former was started with low-frequency mechanical experiments on strongly correlated systems such as polymers at temperatures close to the glass transition one, T_g [1]. It was soon clear that the glass transition phenomenon is characterized — from a spectroscopic point of view — by the freezing of the structural, or α, relaxation, a feature that appears essentially in all susceptibility spectra and that is characterized by a time scale τ_α, which strongly depends on temperature, and which typically changes from $\approx 10^{-13}$ s in the normal liquid phase to $\approx 10^2$ s at the temperature where T_g is conventionally placed. As a matter of fact, one could say that the physics of the glass transition is the physics of the α relaxation, and it is on this last feature that the attention of the spectroscopists has been for long time focused. The urgency of characterizing this process in some detail and on a large temperature range (and consequently on a large time scale) has pushed the experimentalists to develop spectroscopic techniques that could give information both on different dynamical variables and on broader and broader frequency ranges. In this ''expansion'' process, clearly, the field of the glass transition has somehow merged with the study of the atomic dynamics in liquids and also with the classical problem of the classification of liquids. This process is more evident in the high-frequency studies. In fact, while in the supercooled liquid at low frequencies the structural relaxation is by far the dominant one, at high frequencies it frequently occurs on a time scale comparable to that of secondary processes. The study of the nature of these latter processes, of their different occurrences both in differently structured liquids and in different spectroscopic probes, and of their interplay with the structural process is thus a very interesting and timely research field that aims, on one side, at the classification of liquids based on their high-frequency properties and, on the other side, at the understanding of the structural relaxation at temperatures where it occurs on a very fast time scale and, nevertheless, already appears as a precursor of the glass transition.

Besides these considerations, the study of the connection between the glass transition and the high-frequency dynamics has been much stimulated by the development of the mode coupling theory (MCT) [2]. This theory, which has been originally worked out for the density-density correlation function of simple liquids and is currently being generalized to the rotational dynamics as well [3], describes the occurrence of the α-relaxation in terms of a nonlinear coupling of density fluctuation modes via retarded feedback, and predicts, asymptotically, the temperature (or density) evolution of this process toward an ergodic-to-nonergodic transition temperature T_c, where a dynamical singularity is located [2]. The MCT also predicts spectral details of the frequency range that immediately follows the structural relaxation peak in the susceptibility spectra. This additional range, known as the β region, and a whole set of predictions on its evolution with temperature on approaching T_c, constitutes the MCT link between the glass transition phenomenon and the high-frequency dynamics.

Several experimental techniques have been used to verify the MCT predictions on several systems, mainly molecular glass formers [4]. In this connection, Brillouin light scattering is, in principle, an interesting experimental technique both because it directly probes the density correlator and because it has access to an almost two decades spectral window that should just cover the β region [5]. Actually, a fast relaxation dynamics in Brillouin spectra measured in the frequency domain has been observed in several glass formers

[6,5,7–15], but its interpretation within the MCT framework still does not rely on a firm and general data analysis procedure. This observation folds immediately back onto the questions of how to define the liquids that are ''spectroscopically simple'' and thus suited for a comparison with theories such as MCT, and of how differently different dynamical variables reflect the underlying atomic dynamics. These questions represent the main motivation for the present paper that — based on a Brillouin light scattering experiment on the fragile glass former orthoterphenyl (OTP) — aims to present our recent findings on these topics.

The system chosen in this study, OTP, has received much attention by the scientific community studying the glass transition since it is considered as a prototype of the non-associative glass formers. For what concerns the large-wavelength density fluctuation modes — which are the dynamical variables of direct interest here — several experimental techniques have been employed: ultrasonic measurements in the low-frequency (MHz) range have reported on the adiabatic speed of sound [16,17]; homodyne light beating spectroscopy has been used to characterize the structural relaxation close to T_g [18,19]; Brillouin light scattering experiments have reported on the sound dispersion and absorption in the gigahertz frequency range across T_g [20–22,12]. These latter studies, though informative, are, however, not at all conclusive since only a careful line-shape analysis of the Brillouin spectrum over a large frequency range allows one to investigate in detail the atomic relaxational dynamics [14]. In this spirit, and profiting from the instrumental resources that are nowadays available [23], we have collected high-resolution Brillouin spectra covering nearly two decades in frequency in a wide temperature range across the glass transition, and we have performed a line-shape analysis of the measured spectra. The results of this analysis in the glassy phase have been separately published [13], and give evidence of a ''fast'' relaxational dynamics on the 10^{-11} s time scale. This fast dynamics has then been discussed in a successive paper [24], where it has been shown that it has very likely an intramolecular origin, at least in OTP, and thus that it has no connection with the β region predicted by the MCT in simple systems [2]. Starting from these considerations, we will present here the results of a line-shape analysis of the Brillouin spectra collected in the whole temperature range covering both the glass transition region and the normal liquid range. This analysis is based on a simple phenomenological ansatz for the relaxational dynamics, and is able both to account for the characteristics of the structural relaxation in a way consistent with the other available data [16–19,25], and to give an independent characterization of the fast relaxation. This latter one comes out both to be thermally activated with an activation energy $E_a^f = 0.28 \pm 0.08$ kcal/mol, and to merge with the structural relaxation around the melting temperature T_m.

The paper is organized as follows. In Sec. II we discuss some theoretical aspects that are relevant for what follows and, in particular, we introduce the generalized hydrodynamic model that we use to line-shape analyze the spectra. In Sec. III, we describe the Brillouin light scattering experiment in some detail, and we discuss how to obtain $S(q,\omega)$ on an absolute scale starting from the measured spectra. In the following section (IV) we present a simple discussion of the measured spectra based on the classical acoustic properties, namely, the dispersion and the absorption of the sound waves; then we proceed to the full line-shape analysis, and we present the results that we derive from it. These results are then discussed in Sec. V, paying particular care to the comparison with the other existing data, and our final conclusions are summarized in Sec. VI.

II. THEORETICAL BACKGROUND

In Sec. II A, we briefly recall how the dynamic structure factor $S(q,\omega)$ can be obtained from a light scattering experiment. In Sec. II B we introduce the simple generalized hydrodynamic formalism that is often used to describe the atomic dynamics in terms of the memory function, $m(t)$. Additional discussion of these topics can be found in well-known monographs [26–28]. Finally, in Sec. II C we will introduce the phenomenological model for $m(t)$ that we will use in the full line-shape analysis discussed in Sec. IV.

A. The light-scattering cross section

An ideal light scattering experiment can be schematized as follows: a monochromatic beam of radiation (the probe) with angular frequency (wave vector, polarization) ω_i ($\mathbf{k}_i$, $\mathbf{e}_i$) impinges on a sample (the target) composed of N scattering centers and the radiation with frequency (wave vector, polarization) ω_f ($\mathbf{k}_f$, $\mathbf{e}_f$) scattered at an angle ϑ with respect to the incident beam is detected within a solid angle $\Delta\Omega$ and in a bandwidth $\Delta\omega$. The scattering cross section, far from any resonance, can be written as [26]

$$\frac{\partial^2\sigma}{\partial\omega\partial\Omega} = \frac{\omega_i\omega_f^3}{2N\pi c^4} \sum_{\alpha\beta\gamma\delta} e_i^\alpha e_f^\beta (e_i^\gamma)^* (e_f^\delta)^* \times \int_{-\infty}^{+\infty} dt e^{i\omega t} \langle \tilde{P}_{\alpha\beta}(\mathbf{q},t) \tilde{P}^*_{\gamma\delta}(\mathbf{q},0) \rangle. \quad (1)$$

Here c denotes the speed of light, and the exchanged wave vector is defined as $\mathbf{q} = \mathbf{k}_f - \mathbf{k}_i$; its modulus is fixed by the kinematics of the process that imposes, with high accuracy due to the small value of $(\omega_f - \omega_i)/\omega_i$, the following relation:

$$q = \frac{4\pi n}{\lambda} \sin(\vartheta/2). \quad (2)$$

Here n is the refractive index and λ the wavelength (in vacuum) of the involved photons.

In Eq. (1), $\tilde{P}_{\alpha\beta}(\mathbf{q},t)$ is the space Fourier transform of the total polarizability tensor, i.e.,

$$\tilde{P}_{\alpha\beta}(\mathbf{q},t) = \int d\mathbf{r} e^{-i\mathbf{q}\cdot\mathbf{r}} \left(\sum_{l=1}^{N} \tilde{\alpha}^l_{\alpha\beta}(\{\mathbf{R}_i(t)\}) \delta(\mathbf{r} - \mathbf{R}_l(t)) \right) = \sum_{l=1}^{N} \tilde{\alpha}^l_{\alpha\beta}(\{\mathbf{R}_i(t)\}) e^{-i\mathbf{q}\cdot\mathbf{R}_l(t)}, \quad (3)$$

where $\tilde{\alpha}^l_{\alpha\beta}(\{\mathbf{R}_i(t)\}_{i=1..N})$ is the effective polarizability tensor of the lth molecule, which is a true many-body property that depends on the position $\mathbf{R}_i(t)$ of all the molecules in the target. This quantity can be expressed as

$$\tilde{\alpha}^l_{\alpha\beta} = \alpha\delta_{\alpha\beta} + \beta^l_{\alpha\beta} + (\Delta\tilde{\alpha})^l_{\alpha\beta}, \tag{4}$$

where $\alpha^l_{\alpha\beta} = \alpha\delta_{\alpha\beta} + \beta^l_{\alpha\beta}$ is the bare polarizability, with α being its isotropic component and $\beta^l_{\alpha\beta}$ its traceless component; and where $(\Delta\tilde{\alpha})^l_{\alpha\beta}$ is the many-body renormalization contribution.

The first, isotropic (ISO) term in Eq. (4), α, does not depend on the molecular coordinates and its self-correlation function contributes to Eq. (1) through

$$\left[\frac{\partial^2\sigma}{\partial\omega\partial\Omega}\right]_{ISO} = \frac{\omega_i\omega_f^3}{2N\pi c^4}\alpha^2|\mathbf{e}_i\cdot\mathbf{e}_f^*|^2\cdot\int_{-\infty}^{+\infty}dt e^{i\omega t}\langle\rho_{\mathbf{q}}(t)\rho_{\mathbf{q}}^*(0)\rangle, \tag{5}$$

where $\rho_{\mathbf{q}}(t)$ is the $\mathbf{q}$ component of the microscopic molecular center-of-mass number density, $\rho(\mathbf{r},t)$.

Thus, the isotropic polarizability contributes to the scattering cross section through a term proportional to the dynamic structure factor $S(q,\omega)$ defined as

$$S(q,\omega) = \int_{-\infty}^{\infty}dt e^{-i\omega t}\langle\rho_{\mathbf{q}}(t)\rho_{\mathbf{q}}^*(0)\rangle. \tag{6}$$

This term does not appear in the fully depolarized configuration, i.e., when $\mathbf{e}_i\perp\mathbf{e}_f$.

The second term in Eq. (4), $\beta^l_{\alpha\beta}$, only depends on the orientational degrees of freedom, while the third term $(\Delta\tilde{\alpha})^l_{\alpha\beta}$ mainly arises, in simple molecular systems such as OTP, from the renormalization effects on the bare polarizability of the lth molecule coming from the local electromagnetic fields produced by the multipoles of the other molecules of the system. These multipoles, in turn, are induced both by the external field (probe) and by the local electromagnetic field. To first order in the deviation of the local field from the external one, and in the further hypothesis of an almost symmetrical bare polarizability ($\|\beta\| \ll \alpha$), the result for the effective polarizability is [29]

$$\Delta\tilde{\alpha}^l_{\alpha\beta}(\mathrm{DID}) = \alpha^2\sum_{l\neq l'}T^{(2)}_{\alpha\beta}(l,l'), \tag{7}$$

which is known as the pure dipole-induced dipole (DID) contribution to the renormalized polarizability. Here, $T^{(2)}(l,l')$ represents the usual dipole propagator [26,29].

The two tensors $\beta^l_{\alpha\beta}$ and $\Delta\tilde{\alpha}^l_{\alpha\beta}(\mathrm{DID})$, both of which are traceless, second rank tensors, contribute on an almost equal footing to the scattered light when molecules such as OTP are considered, as can be evaluated from molecular dynamics simulation [30]. Moreover, as a general consideration, they both give rise to two different spectral features: one q independent and the other q dependent. The q-independent one appears in the spectra, on a qualitative ground, as a smooth band with a temperature-dependent width and with tails that extend up to at least few terahertz, i.e., up to the frequency range where the optical bands appear in most of the organic liquids. This contribution is fully depolarized, i.e., the ratio r (depolarization ratio) of its intensity in the depolarized configuration ($\mathbf{e}_i\perp\mathbf{e}_f$) to the intensity in the polarized one ($\mathbf{e}_i\|\mathbf{e}_f$) is fixed and equal to 0.75. The q-dependent spectral feature gives rise, in turn, to two different contributions. The first contribution reflects the transverse dynamics in the supercooled liquid and glassy phases [31,29]. This contribution is forbidden by a selection rule in the polarized spectrum and its intensity in the depolarized spectrum depends on the scattering angle, being zero in the backscattering ($\theta = 180°$) geometry [32]. The second q-dependent contribution, conversely, gives essentially rise, in the supercooled liquid and glassy phases, to a feature that reflects the longitudinal dynamics and adds up to the isotropic spectrum, as it has been recently underlined [33]. The contribution of this second feature to the isotropic spectrum can be directly evaluated by comparing the longitudinal Brillouin peaks in the 90° geometry as measured in the vertical-vertical (VV) and horizontal-horizontal (HH) polarization configurations [34]. In organic liquids such as OTP, fortunately, this contribution comes out to be safely negligible [34]. Consequently, by measuring light scattering spectra in the depolarized and polarized configurations, by multiplying the former by 0.75 and then by subtracting the former from the latter, the dynamic structure factor can be obtained.

It has to be pointed out that among all the possible induction mechanisms, the (pure) DID (which is, however, by far the dominant one in nonionic systems) gives rise to a pure, second rank, renormalized polarizability tensor. It is possible, however, that other induced effects, each with its peculiar spectral shape, affect the polarized and depolarized spectra in a different fashion: r can be no longer 0.75 and, moreover, it can also be frequency dependent. If this is the case, obviously, the previously discussed procedure to determine the $S(q,\omega)$ spectrum from the polarized and depolarized ones becomes unreliable. Only a careful experimental analysis of the polarized and depolarized spectra can establish whether the other-than-DID induced effects, with their eventual isotropic component, are effectively active in the system under examination.

Summarizing, in molecular liquids the polarized Brillouin spectrum in the backscattering configuration, $I_{\|}$, is, to a good approximation, the sum of a q-dependent isotropic term I_{ISO}, proportional to the $S(q,\omega)$ and of a q-independent anisotropic contribution $I_{\perp}$, while the fully depolarized spectrum consists only of the latter contribution. It is always possible to derive the isotropic spectrum as

$$I_{ISO} = I_{\|} - r^{-1}I_{\perp}, \tag{8}$$

where r is the depolarization ratio. The $S(q,\omega)$ contribution to $I_{\|}$ goes to zero at frequencies higher than the Brillouin peak ($\approx$40 GHz for fragile glass formers such as OTP), so that one can check whether, above this limit, the $I_{\|}$ and $I_{\perp}$ spectra have the same shape and whether the direct measurement of r actually gives 0.75. If this is the case, one can

reasonably assume that the isotropic induced effects have a negligible weight and that the I_{ISO} spectrum is actually proportional to the $S(q,\omega)$ one.

B. The dynamic structure factor

In order to simplify the expressions that follow, we introduce the normalized correlation function of the density fluctuations:

$$\Phi_q(t)=\frac{\langle \delta\rho_q^*(0)\,\delta\rho_q(t)\rangle}{S(q)}, \tag{9}$$

where $S(q)$ is the static structure factor

$$S(q)=\langle \delta\rho_q^*(0)\,\delta\rho_q(0)\rangle=\frac{1}{2\pi}\int_{-\infty}^{\infty} d\omega S(q,\omega). \tag{10}$$

This corresponds to the zeroth moment of the dynamic structure factor, $M_S^{(0)}$. In the low-q limit appropriate for light scattering experiments, the following relation holds [27]:

$$M_S^{(0)}=S(q\to 0)=\frac{\rho k_B T\chi_T}{M}, \tag{11}$$

where M is the mass of the scattering unit (the molecular mass of OTP, in the present case), k_B the Boltzmann constant, ρ the mass density, and χ_T the isothermal compressibility. We also quote the second (nonzero) moment of $S(q,\omega)$, which is given by the relation:

$$M_S^{(2)}=\frac{1}{2\pi}\int_{-\infty}^{\infty} d\omega\omega^2 S(q,\omega)=\frac{q^2 k_B T}{M}. \tag{12}$$

An equation of motion for $\Phi_q(t)$ can be written in the form of a generalized Langevin equation [27,28]:

$$\frac{\partial^2\Phi_q(t)}{\partial t^2}+\omega_T^2(q)\Phi_q(t)+\int_0^t dt' m_q(t-t')\frac{\partial\Phi_q(t')}{\partial t'}=0. \tag{13}$$

Here, $\omega_T(q)$ is the ratio of the first two nonzero spectral moments, namely, $\omega_T^2(q)=M_S^{(2)}/M_S^{(0)}$. Moreover, we have introduced the second memory function $m_q(t)$ of the Zwanzig-Mori expansion of $\Phi_q(t)$ [35]. Analogously, in the frequency space, the dynamic structure factor can be written, using Eqs. (6) and (13), as

$$S(q,\omega)=\frac{2v_o^2q^2}{\omega}\mathrm{Im}[\omega^2-\omega_T(q)^2-i\omega m_q(\omega)]^{-1}, \tag{14}$$

where Im denotes the imaginary part, and $v_o^2=(k_BT)/M$. From a practical point of view, Eqs. (13) and (14) can be simply considered as equations that define $m_q(t)$. The advantage of Eqs. (13) and (14) is that the introduction of simple models for $m_q(t)$ — instead of introducing them directly for $\Phi_q(t)$ — guarantees that at least the first two nonzero spectral moments of $S(q,\omega)$ are respected. At this stage Eqs. (13) and (14), being formal expressions, correctly describe the atomic dynamics at any time or frequency, and wave vector.

Formally, the general situation typical for Brillouin light scattering where the continuum approximation still holds but relaxational effects have to be taken into account can be handled by retaining the formal structure of the hydrodynamic equations, but replacing the transport coefficients with functions that can vary in time (or frequency). This is the so-called generalized hydrodynamic approach [27], where the memory function is written as

$$m(t)=\omega_T^2[\gamma-1]e^{-D_Tq^2t}+K_l(t). \tag{15}$$

Here $\gamma=C_P/C_V$ is the constant pressure to constant-volume specific-heat ratio; $D_T=\kappa/(\rho C_V)$, where κ is the thermal conductivity; $\omega_T^2=\omega_T^2(q\to 0)=q^2c_0^2/\gamma$, where c_0 is the adiabatic sound velocity; and $K_l(t)$ is the longitudinal kinematic viscosity function [27]. On the right-hand side (rhs) of Eq. (15), the first term describes the thermal diffusion process, while the second term contains the relevant relaxational dynamics. This latter term is related to the kinematic longitudinal viscosity, ν_l, by the simple condition

$$\int_0^\infty dtK_l(q,t)=q^2\nu_l. \tag{16}$$

In addition to Eq. (16), further constraints could be imposed on $K_l(t)$ by the knowledge of higher spectral moments. However, for the sake of the present data analysis, it is not much useful to go beyond the second spectral moment of $S(q,\omega)$.

In principle, the longitudinal kinematic viscosity function is the sum of a bulk and of a shear contribution; moreover, the latter contribution can be also modified, in the case of anisotropic molecules such as OTP, by the coupling between the traceless part of the polarizability and the molecular center-of-mass translation [36]. However, the analysis of the light-scattering isotropic spectra alone cannot really discriminate among these different contributions, and thus we will simply introduce, in the next paragraph, a phenomenological model for the average relaxation processes that directly affect the longitudinal kinematic viscosity function.

C. Choosing the model for $K_l(\omega)$

The first obvious ingredient of a model for $K_l(\omega)$ is the structural relaxation, which is the ubiquitous process accompanying the glass-transition [37]. This process, which is generally non-activated and cooperative in nature, as indicated by the high values of the (temperature-dependent) activation energy, is, in time domain, generally described in terms of a stretched exponential whose Fourier transform is well approximated by the Cole-Davidson function [38]

$$K_l^{CD}(\omega)=q^2\Delta_\alpha^2(i\omega\rho)^{-1}[1-(1+i\omega\tau_\alpha)^{-\beta_{CD}}].$$

Here Δ_α^2 is the relaxation strength; β_{CD} is the stretching coefficient, whose value ranges between 0 and 1; and τ_α is the structural relaxation time.

The structural process is by far the dominant process in the kHz to MHz range, as e.g., shown in the ultrasonic literature [39,37]. However, this is no longer the case in the GHz frequency range probed by Brillouin light scattering, since the existence of a fast relaxation channel has been clearly identified in several glass formers including $GeSBr_2$ [6], $CaKNO_3$ (usually called CKN) [5], propylene carbonate [7], As_2O_3 [9], polybutadiene [8,10], *m*-TCP [11], epoxy resin [14], and *m*-toluidine [15]. The question that is still debated is, conversely, what is the correct way to analyze this additional contribution. In this regard, two main strategies have essentially been followed. The first one is phenomenological in spirit [6,8,11,13,14], and relies (i) on the description of this additional process in terms of an additional contribution to the memory function and (ii) on the choice of reasonable constraints on the fitting parameters in order to get to reliable results. The second strategy [5,7,10,15], conversely, relies on the MCT ansatz for the memory function; the fast process is then described as the superposition of the β-region predicted by MCT and the microscopic dynamics.

For what concerns this latter approach, a first detailed study was performed on CKN [5]. In that case, the coincidence of the relaxation times as derived from the isotropic and the depolarized light scattering spectra was used to infer the strong similarity between the depolarized spectrum and the memory function governing the dynamic structure factor [5]. Exploiting this argument, and thus relying on an independent ansatz for the memory function, the shape of the Brillouin spectra of CKN was successfully analyzed, showing consistency to the MCT predictions [5]. Unfortunately, in all other studied glass formers, the relaxation times derived from the isotropic and the depolarized light scattering spectra are clearly different, and the preceding argument can no longer be exploited. Nevertheless, consistency between the MCT predictions and the isotropic spectra has successively been looked for, with either an ambiguous answer due to the strong correlation of the free-fitting parameters [7,15], or with a negative answer due to the presence of additional relaxation processes not yet included in MCT [10].

For what concerns the first, phenomenological approach, different strategies have been used in order to constrain somehow the free-fitting parameters, and different results for the fast dynamics have been obtained. For example, in a study on the $GeSBr_2$ glass former [6], Loheider *et al.* used a two-relaxations-based phenomenological memory function in the shape analysis of their Brillouin spectra, with an additional constraint coming from the global fit of spectra measured at different q's. The need for a fast contribution in the memory function was thus shown. However, this fast process was modeled in terms of a completely relaxed ansatz, corresponding to a fast relaxation time out of the Brillouin window, and thus it was not possible to fully characterize it. In a successive study of an epoxy resin [14], as it had been done in the case of CKN [5], Fioretto *et al.* have exploited the similarity between the low-frequency portion of the isotropic light-scattering spectra and the dielectric relaxation spectra in motivating the use of these latter ones as an ansatz for the memory function. In that case, the Brillouin spectra have been successfully fitted, and consequently the fast process found in the isotropic spectra has been associated with the one present in the dielectric spectra and, as such, has been attributed to the rotation of a specific group of the resin [14]. In a more recent study on the fragile glass former *m*-TCP [11] Soltwisch *et al.* have again used a two-relaxations-based phenomenological memory function, with additional constraints coming from the global fit of spectra measured with different polarizations and from acoustic dispersion and absorption data measured at lower frequencies. The results of this analysis have been compared with the MCT predictions, and a qualitative agreement in several important points has been obtained [11].

For what concerns OTP, it has already been shown that the isotropic Brillouin spectra collected in the glassy phase are affected by a fast relaxational dynamics on the 10^{-11} s time scale [13]. The nature of this dynamics has been successively addressed [24], and it has been shown that (i) the same fast relaxation that is observed in the glassy phase of OTP actually is also present in the single crystal, and that (ii) it affects the longitudinal dynamics but not the transverse one. From these indications, it has been concluded that, at least in the isotropic Brillouin spectra of OTP, this fast dynamics very likely has an intramolecular origin, i.e., it comes from the coupling of the acoustic waves to one or more intramolecular degrees of freedom [24] and that consequently it has no connection with the β region predicted by the MCT in simple systems [2]. We want to underline that the presence of similar secondary, fast relaxations has been recognized since a long time, in particular by people using ultrasonics to study the dynamics of normal liquids, as shown by the extensive work described by Herzfeld and Litovitz [39].

Given these results, we use here a phenomenological approach to describe our isotropic Brillouin spectra, and we model the contribution of the fast dynamics in terms of a relaxational process in addition to the structural one. Moreover, in order to minimize the number of parameters, we describe this contribution in terms of a simple Debye process:

$$K_l^{fast}(\omega)=q^2\Delta_f^2\tau_f\rho^{-1}(1+i\omega\tau_f)^{-1},$$

where Δ_f^2 is the (fast) relaxation strength, and τ_f is the relaxation time. Finally, in order to be able to describe, at the same time, also the $S(q,\omega)$ spectra measured at high q with Brillouin x-ray scattering [25,13], an additional contribution will be added that is thought to be so fast to be well represented in the gigahertz frequency range by a term constant in frequency (instantaneous in time), $K_l^{inst}(\omega)=\gamma_0 q^2$. Conceptually, this last process is related to fast molecular motions which induce a lost of correlation at very early stages, usually on the 10^{-13} s time scale. To keep consistency with the current language used in the literature on glass-forming liquids, we will refer to this contribution as to the microscopic or instantaneous decay [2]. In total, our model reads:

$$K_l^{<}(\omega)=\frac{q^2\Delta_\alpha^2}{i\omega\rho}\left[1-\frac{1}{(1+i\omega\tau_\alpha)_{CD}^{\beta}}\right]+\frac{q^2\Delta_f^2\tau_f}{\rho(1+i\omega\tau_f)}+\gamma_0 q^2. \tag{17}$$

This model, apart from the initial instantaneous decay, describes a two steps relaxation process at those temperatures where $\tau_\alpha \gg \tau_f$, and thus — since $(\tau_f)^{-1}$ is in the gigahertz frequency range — it is expected to hold around and below the melting temperature. In particular, it is expected to hold also in the glassy phase, though with the following caveat: (i) the structural relaxation is now frozen, and thus it contributes only through its limiting real part $K_{l,\infty}^{CD}(\omega) = q^2\Delta_\alpha^2(i\omega\rho)^{-1}$; (ii) the simple approximation of the contribution of all the residual harmonic and anharmonic processes through the Markovian term $K_l^{inst}(\omega) = \gamma_0 q^2$ may become insufficient at low temperatures, where additional relaxational-like processes may enter the Brillouin spectral window, as observed in other systems [40]. However, we will not discuss this latter temperature region, and thus we will keep our simple Markovian approximation.

In the model Eq. (17), the Brillouin position is $\omega_0 = qc_0$ at temperatures where $\omega_p\tau_\alpha(T) \ll 1$ (ω_p is the frequency position of the Brillouin peak); it crosses to an intermediate level $\omega_{\infty\alpha}$ at temperatures such that $\omega_p\tau_\alpha(T) \gg 1$ and contemporarily $\omega_p\tau_f(T) \ll 1$; and eventually it crosses to an ''upper'' level ω_∞ at temperatures such that $\omega_p\tau_f(T) \gg 1$. Moreover, the strengths of the two considered relaxations, Δ_α^2 and Δ_f^2, are related to ω_0, $\omega_{\infty\alpha}$, and ω_∞ through the relations

$$\Delta_\alpha^2 = \rho q^{-2}(\omega_{\infty\alpha}^2 - \omega_0^2), \tag{18}$$

$$\Delta_f^2 = \rho q^{-2}(\omega_\infty^2 - \omega_{\infty\alpha}^2). \tag{19}$$

As we will show in Sec. IV, the characteristic time scales of the structural and of the fast relaxation, which are completely different around T_g, get closer and closer when increasing the temperature. Actually, at some temperature T^* in the normal liquid phase τ_α and τ_f get so close that it is no longer possible to really discriminate between them. At temperatures higher than T^* it is reasonable to expect that the two processes merge in a single one, a circumstance that is usually met in the study of glass forming liquids. This conceptual expectation meets the technical need of simplifying as much as possible the memory function at $T > T^*$ since, due to the softening of the elastic moduli in the normal liquid phase, the relaxation region that is directly probed in a light scattering experiment at frequencies below the Brillouin peak becomes smaller and smaller, and thus the spectra become more and more unable to discriminate among different models. At temperatures above T^*, then, a simple single-relaxation, Debye model will be used, i.e.,

$$K_l^>(\omega) = \frac{q^2\Delta^2\tau}{\rho(1 + i\omega\tau)} + \gamma_0 q^2, \tag{20}$$

where Δ^2 and τ are the relaxation strength and relaxation time of this final process. In the model Eq. (20) the Brillouin position is ω_0 at temperatures where $\omega_p\tau(T) \ll 1$ and it crosses directly to ω_∞ at temperatures such that $\omega_p\tau(T) \gg 1$. As before, the strength of the final relaxation, Δ^2, is related to ω_0 and ω_∞ through the relation

$$\Delta^2 = \rho q^{-2}(\omega_\infty^2 - \omega_0^2). \tag{21}$$

III. EXPERIMENTAL RESULTS

In the present study, OTP of 99% purity purchased from Aldrich Chemicals has been used. Two different samples were prepared. The first one was purified by repeated recrystallizations in methanol solutions, filtered through a 0.22-μm teflon filter at a temperature of about 350 K and distilled under vacuum directly in the suprasil rectangular cell ($2 \times 10 \times 40$ mm^3) used for the measurements. The cell was sealed without breaking the vacuum. The second sample was kept at about 430 K for several hours, slowly degassed and filtered as described above in a cylindrical pyrex cell (inner diameter $\approx$ 1 cm). Both procedures gave samples of good optical quality and no difference has been observed in their spectra in the whole measured frequency range between 4 and 60 GHz. For this reason, no indication will be given in the following about which sample was used for each measurement.

Brillouin spectra were collected in the temperature range 110–600 K, that is comprising the whole liquid — normal and supercooled — phase (boiling point, $T_b \simeq 610$ K; melting point, $T_m = 329$ K) down to the glass ($T_g = 244$ K). The samples were placed in a copper holder that was used to regulate the temperature. For the measurements above room temperature, the sample holder was heated with a NiCr wire using a conventional dc power supply; for the low-temperature measurements, it was cooled by fluxing liquid air in a copper tube fused around the holder. In both cases, the temperature was controlled by a Thor Cryogenics 3010 II model temperature controller and measured by a Pt100 calibrated resistance placed close to the sample. The temperature fluctuations were kept within ± 0.1 K during the spectra recording and each measurement was begun after the sample temperature was thoroughly equilibrated. The sample temperature was varied with a typical 0.5 °C/min rate, and no spectral changes were observed among different scans on cooling or heating the sample.

A Coherent-Innova 300 model Ar^+ laser was operated with a typical power of $\approx$300 mW on a single mode of the $\lambda_0 = 514.5$ nm line. The light scattered by the sample was analyzed by means of a Sandercock-type (3+3)-pass tandem Fabry-Perot interferometer characterized by a finesse of about 100 and a contrast $> 5 \times 10^{10}$ [23]. The elastic scattering from a dilute aqueous suspension of latex particles (120 nm diameter) was used to determine the instrumental resolution function $R(\omega)$. A 0.5-nm bandwidth [half width at half maximum (HWHM)] filter was used to suppress the signal from high interference orders transmitted by the frequency analyzer. Both polarized ($I_\parallel$) and depolarized ($I_\perp$) Brillouin spectra were collected in the back-scattering ($\theta = 180°$) geometry that, as discussed in Sec. II, is the best suited for determining the $I_{ISO}(\omega)$ spectrum via Eq. (8). In order to obtain high-resolution spectra sufficiently extended in frequency, for each temperature and polarization we joined two spectra collected with different free spectral range (FSR): 30 GHz and 10−11 GHz, depending on the temperature. The integration time was of $\approx$10 s/channel and the effect of the dark counts (<1 count/s) was checked to be negligible.

Typical polarized and depolarized spectra obtained in this

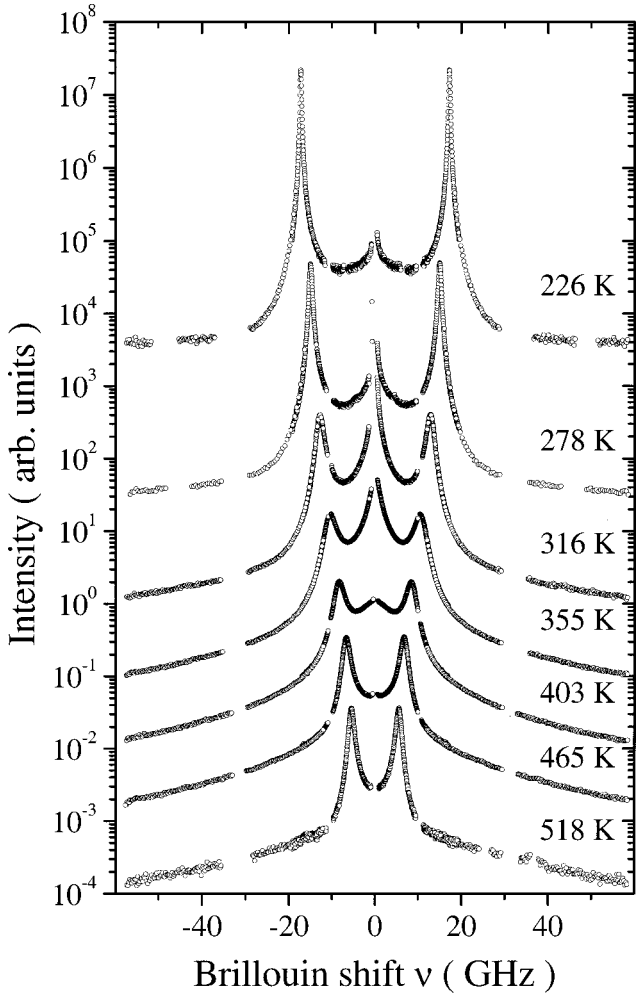

FIG. 1. Polarized Brillouin light scattering spectra at the indicated temperatures. Each spectrum is obtained by overlapping two spectra measured with a FSR of 10−11 GHz (depending on the temperature) and 30 GHz. The holes in the spectra correspond to the position of the instrumental ghosts.

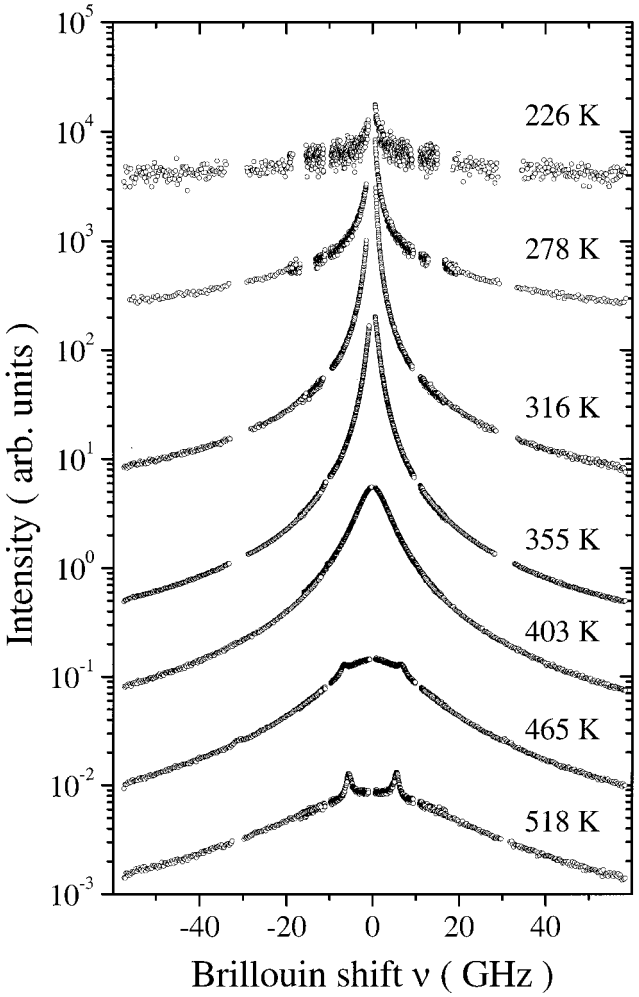

FIG. 2. Depolarized Brillouin light scattering spectra at the indicated temperatures. Each spectrum is obtained by overlapping two spectra measured in the same conditions as the corresponding polarized ones. The holes in the spectra correspond to the position of the instrumental ghosts.

way in the frequency range 0.4−60 GHz are presented in Figs. 1 and 2, respectively. The holes in the spectra correspond to the position of the experimental ghosts; their presence, however, does not affect the overall shape of the spectra due to the high contrast of the Sandercock-type interferometer. Moreover, by using different FSRs and pinhole sizes, we have checked that the presented spectra are unaffected by the elastic stray light coming from spurious reflections. Figures 1 and 2 show that, in the liquid range, the anisotropic scattering sensibly contributes to the shape of the polarized spectrum, particularly at frequencies lower than the Brillouin peak position. In the frequency region of the Brillouin peaks and at temperatures close to and lower than T_g, in turn, the polarized spectra are in good approximation equal to the isotropic ones. For the determination of the sound speed and absorption, to be discussed in Sec. IV, the peak position and the full width at half maximum (FWHM) of the Brillouin components are the only relevant parameters and thus, for this purpose, at some temperatures only polarized spectra were collected.

At selected temperatures, more extended $\parallel$ and $\perp$ spectra were collected using a SOPRA DMDP2000 monochromator [41] with a 1.5 GHz frequency resolution. These spectra were then joined to the high-resolution ones in order to obtain final spectra extending up to about 300 GHz. As an example of this procedure, Fig. 3 reports the individual spectra collected at $T=297$ K (a) and then joined (b). In the present case, the $I_{\parallel}$ and $I_{\perp}$ spectra have the same shape in a large frequency range, as it is shown in Fig. 4 for the spectra measured at $T=297$ K. It is then possible to determine the $I_{ISO}(\omega)$ spectra simply by overlapping the tails of the $I_{\parallel}$ and $I_{\perp}$ spectra and then subtracting the latter from the former. The isotropic spectra determined in this way are presented in Fig. 5 and cover a spectral window between about 0.4 and 25 GHz. Moreover, the depolarization ratio r of OTP has been carefully measured at $T=297$ K and, as reported in the inset of Fig. 4, shows a frequency-independent value of $r=0.73 \pm 0.03$, consistent — within experimental uncertainties — with the fully depolarized value. It is then reasonable to as-

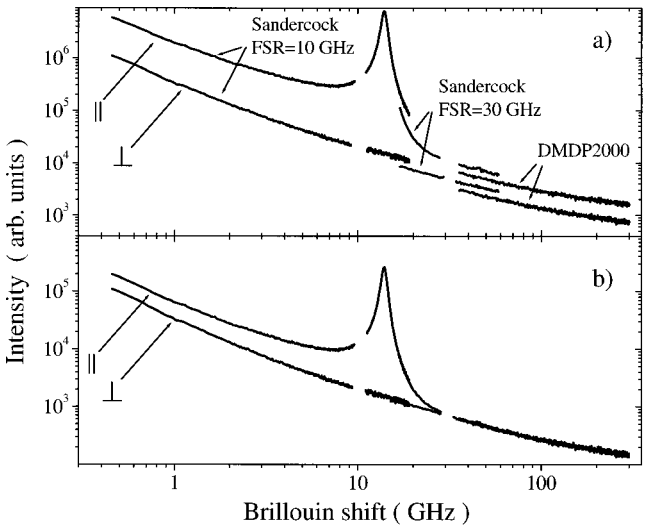

FIG. 3. Polarized and depolarized spectra at 297 K collected using both the tandem Fabry-Perot with FSR of 10 and 30 GHz [left and central curves in (a)] and the SOPRA DMDP2000 monochromator set to 1.5 GHz frequency resolution [right curve in (a)]. These spectra have been joined in order to obtain extended spectra in the frequency range 0.4−300 GHz (b).

sume that the $I_{ISO}(\omega)$ spectra are simply related to the $S(q,\omega)$ ones via:

$$I_{ISO}(\omega)=I_0\int R(\omega')S(k,\omega-\omega')d\omega', \tag{22}$$

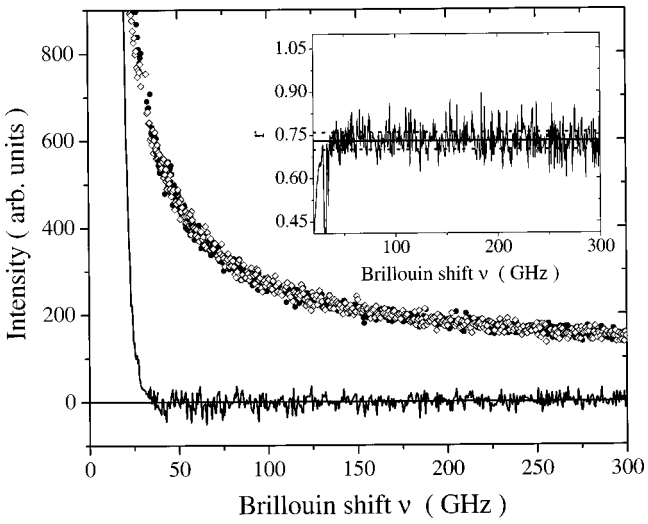

FIG. 4. Tails of the rescaled polarized (full circles) and depolarized (open diamonds) spectra at 297 K obtained by joining spectra collected with different resolutions. Once the depolarized spectra are multiplied by the inverse depolarization ratio, a complete superposition of the shapes is obtained, as emphasized by the isotropic spectrum (full line) going to zero at frequencies higher than about 35 GHz (the Brillouin peak at this temperature is at ≈14 GHz). In the inset, the depolarization ratio r is measured as the ratio of the depolarized to polarized spectra in a frequency range where the isotropic spectrum is expected to give no contribution.

where I_0 is a constant dependent on the scattering cross section and on the experimental setup and $R(\omega)$ is the normalized resolution function. Actually, using a simple procedure based on the knowledge of the first two nonzero spectral moments it is possible to determine I_0, and thus to put the dynamic structure spectra on an absolute scale. In fact, if we indicate with $M_I^{(n)}$ ($M_S^{(n)}$, $M_R^{(n)}$) the nth moment of I_{ISO} ($S(q,\omega)$, $R(\omega)$), the second central moment of the I_{ISO} spectrum, in the general hypothesis of a symmetrical and normalized resolution function, reads:

$$M_I^{(2)}=I_0M_S^{(0)}M_R^{(2)}+I_0M_S^{(2)}. \tag{23}$$

The first term of the rhs of Eq. (23) can be safely neglected since, in the present case, $M_R^{(2)}\ll M_S^{(2)}/M_S^{(0)}=\omega_T^2$. In fact, from the measured (normalized) resolution function, we obtain: $M_R^{(2)}\approx 4\pi^2\times 0.1$ GHz^2. Moreover, for an organic liquid and for a typical light-scattering configuration c_0 ≈1000 m/s, $\gamma\approx 1$, $q\approx 4\times 10^{-2}$ nm^{-1}, and consequently, $\omega_T^2=q^2c_0^2/\gamma\approx 4\pi^2\times 10^3$ GHz^2. Thus, Eq. (23) can be readily used to determine the constant I_0 via the following relation

$$I_0\approx\frac{M}{k_BTq^2}M_I^{(2)}(1+O(10^{-4})), \tag{24}$$

and the computation of the second moments $M_I^{(2)}$ of the isotropic spectra. The result of this procedure is shown in Fig. 5, where we have reported the (resolution convoluted) dynamic structure factor on an absolute scale at different temperatures.

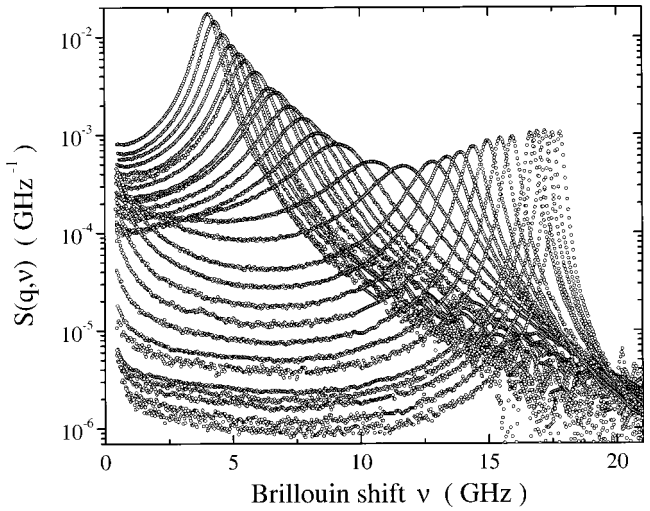

FIG. 5. Dynamic structure factor spectra at the following temperatures (Brillouin peaks from right to left): 185.9, 206, 226, 236.2, 245.2, 259.5, 268.3, 277.8, 287.9, 297.1, 306.8, 316.3, 335.2, 354.8, 381.7, 403, 422.9, 443.4, 464.8, 474.8, 499, 518.2, 529.2, 549.9, 567.2, 586.2, and 602.3 K. The spectra are reported on an absolute scale, obtained using the second moment sum rule of the $S(q,\omega)$.

IV. DATA ANALYSIS

In Sec. IV A, we discuss the classical acoustic information that can be extracted via the frequency position and the linewidth of the Brillouin peaks, namely, the temperature evolution of the hypersonic velocity and attenuation. In Sec. IV B, then, we will present the results of our full line-shape analysis, whose general discussion will be postponed to the next section.

A. Acoustic properties of OTP

The dynamic structure factor spectra of Fig. 5 are essentially characterized by the Brillouin peak, located at the characteristic frequency of the longitudinal-acoustic (LA) modes of OTP, and by a broad band centered at zero frequency and usually referred to as the Mountain mode [42]. The spectral region around the Brillouin peak can be approximately described by a damped harmonic oscillator (DHO) ansatz [43,14]:

$$I_{DHO}(\omega) \propto \frac{2\Gamma_p \omega_p^2}{[\omega_p^2 - \omega^2]^2 + [2\omega\Gamma_p]^2}, \tag{25}$$

where ω_p and $2\Gamma_p$ approximately correspond to the frequency position and to the linewidth (FWHM) of the LA peaks. Equation (25), convoluted with the resolution function, has been fitted to the experimental spectra in a narrow region around the LA peaks, and the obtained values of ω_p and $2\Gamma_p$ are reported in Table I. These parameters are related to the (apparent) velocity of sound $c(\omega)$ and to the (apparent) kinematic longitudinal viscosity $\nu_l(\omega)$ through the relations $c(\omega_p) = \omega_p / q$ and $\nu_l(\omega_p) = 2\Gamma_p / q^2$. In order to derive $c(\omega_p)$ and $\nu_l(\omega_p)$ we need to know q, which we have calculated — as discussed in the following — using the values of the refractive index n and of the mass density ρ. For what concerns the latter, several sets of data are reported in the literature [44–48] covering the whole (supercooled and normal) liquid phase and the glassy phase down to 218 K. For temperatures above and below T_g, respectively, these data can be well represented by

$$\rho(T) = 1.300 - 7.12 \times 10^{-4} T - 1.08 \times 10^{-7} T^2, \tag{26}$$

$$\rho(T) = 1.192 - 2.92 \times 10^{-4} T, \tag{27}$$

with T in K and ρ in g/cm^3. The ρ values in the whole temperature range of interest here have been obtained using these expressions. For what concerns the index of refraction, data are reported in the literature [20,22,49] in the 303–393 K temperature range, and they follow a Clausius-Mossotti relation

$$\frac{n(T)^2 - 1}{n(T)^2 + 2} = \frac{4}{3} \pi \rho(T) p \tag{28}$$

with a (temperature independent) effective optical polarizability $p = 31$ Å^3 [49]. The available data for n have been extrapolated in the whole temperature range of interest here using the same expression.

TABLE I. Peak position (ν_p) and FWHM ($2\Gamma_p$) of the Brillouin peak at the investigated temperatures. These spectral parameters have been determined by fitting the peak region with a simple DHO model, Eq. (25), convoluted with the instrumental resolution. The last column reports the corresponding values of the exchanged momentum q, obtained as discussed in the text.

T (K)	ν_p (GHz)	$2\Gamma_p/2\pi$ (GHz)	q (nm^{-1})
114.5	18.72	0.15	0.042
137.0	18.43	0.13	0.042
166.0	18.07	0.22	0.041
185.9	17.81	0.28	0.041
196.0	17.67	0.26	0.041
206.0	17.50	0.30	0.041
216.0	17.40	0.31	0.041
226.0	17.23	0.33	0.041
236.2	16.91	0.39	0.041
245.2	16.67	0.41	0.041
259.5	15.95	0.56	0.041
268.3	15.49	0.59	0.041
277.8	14.99	0.72	0.041
287.9	14.42	0.91	0.040
297.1	13.92	1.11	0.040
306.8	13.41	1.37	0.040
316.3	12.87	1.72	0.040
335.2	11.80	2.55	0.040
354.8	10.68	3.15	0.039
381.7	9.35	3.04	0.039
403.0	8.58	2.61	0.039
422.9	7.93	2.29	0.038
443.4	7.38	2.02	0.038
464.8	6.84	1.81	0.038
474.8	6.57	1.75	0.038
499.0	6.00	1.47	0.037
518.2	5.59	1.33	0.037
529.2	5.34	1.23	0.037
549.9	5.00	1.17	0.037
567.2	4.67	1.04	0.036
586.2	4.33	0.88	0.036
602.3	4.08	0.86	0.036

The q values of interest here are eventually obtained through Eq. (2), and are reported in Table I. The apparent velocity of sound and longitudinal viscosity obtained using these data are reported in Figs. 6 and 7 (full triangles), and are compared to other literature data. In particular, two sets of ultrasonic data are available, the first referring to ≈ 1 MHz [17] (crossed open circles), and the second to frequencies between 10 and 50 MHz [16] (open triangles). For what concerns Brillouin light scattering data, to our knowledge three previous experiments, all performed in the 90° scattering configuration, are reported in the literature [20–22]. A general good agreement among these results has been observed and therefore we only report the tabulated data of Ref. [21] (converted to velocity data with the same refractive index used above) for comparison purposes (open diamonds).

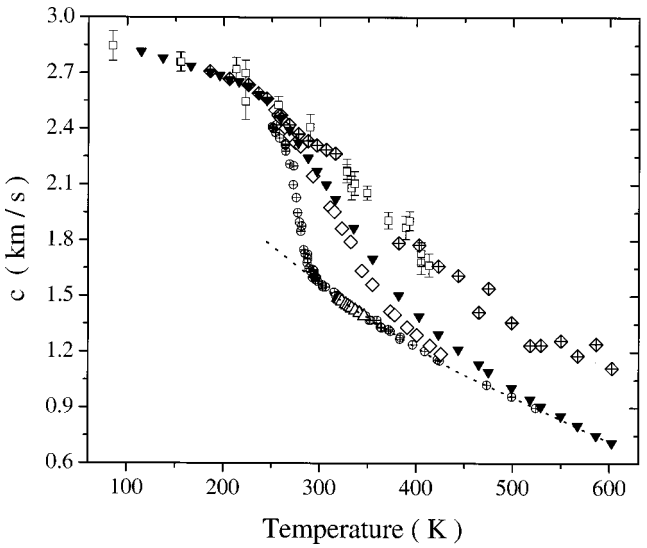

FIG. 6. The sound velocity data from the 180° light scattering experiment presented here (full triangles) compared to literature data: (i) ultrasonic data at ≈ 1 MHz [17] (crossed circles); (ii) ultrasonic data at 10–50 MHz [16] (open triangles); (iii) light scattering data obtained in the 90° geometrical configuration [21] (open diamonds); and (iv) inelastic x-ray scattering data at $q \approx 1$ nm^{-1} [25] (open squares). The dotted line represents c_0, the low-frequency sound velocity from Eq. (32), used in the lineshape fitting analysis. Eventually, the values of $c_\infty(T)$ (crossed diamonds) obtained in this fitting analysis are also reported, showing a good consistency with the x-ray scattering data.

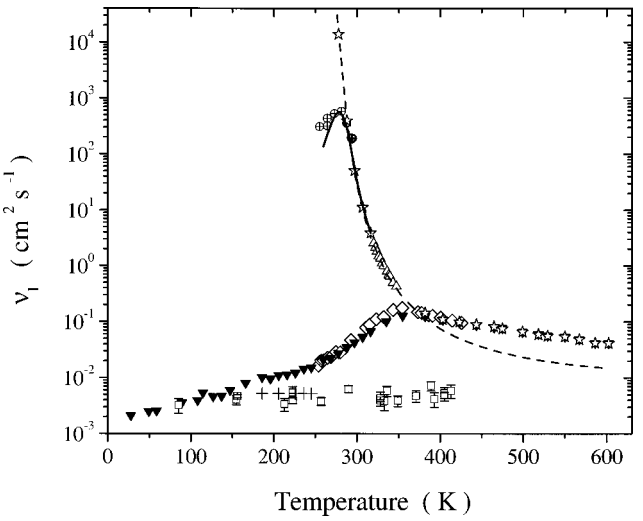

FIG. 7. The apparent longitudinal kinematic viscosity data from the 180° light scattering experiment presented here (full triangles) compared, on a semilog scale, to literature data: (i) ultrasonic data at ≈ 1 MHz [17] (crossed circles); (ii) ultrasonic data at 10–50 MHz [16] (open triangles); (iii) light scattering data obtained in the 90° geometrical configuration [21] (open diamonds); and (iv) inelastic x-ray scattering data at ≈ 1 nm^{-1} [25] (open squares). The *globally* fitted results for the unrelaxed longitudinal kinematic viscosity obtained from the instantaneous memory term in the line-shape fitting analysis discussed in Sec. IV are also reported (pluses), showing good consistency with the x-ray scattering results. The dashed line is the longitudinal kinematic viscosity obtained from the 10–50 MHz absorption data [16] and extrapolated in the whole temperature range as $4\nu_s$. This extrapolation agrees well in the supercooled phase with the determination of the longitudinal kinematic viscosity obtained from the line-shape fitting analysis discussed here (open stars). Finally, as a further consistency check, the apparent longitudinal kinematic viscosity at 1 MHz calculated from the model used in the line-shape fitting analysis is also reported (full line), and is found to be consistent with the corresponding experimental ≈ 1 MHz ultrasonic data.

Eventually, Brillouin x-ray scattering data referring to $q \approx 1$ nm^{-1} [25] are also reported (open squares).

From a very general point of view, these data show the well-known characteristics expected in presence of the structural relaxation process. In fact, the velocity changes from a low temperature trend, toward a S-shaped relaxation region, to a relaxed high-temperature trend and the longitudinal viscosity presents a peak in the temperature range where the relaxation is active and reaches quite small values both in the normal liquid and in the glassy phase. Moreover, the region of strong interaction with the relaxation, where the velocity data cross from a low- to a high-temperature level and where the longitudinal viscosity data present a maximum, shows the usual shift toward lower temperatures when lowering the probing frequency: this trend can be followed from the ultrasonic data to the 90° and 180° light scattering ones. In the x-ray scattering data, eventually, the probing frequency is so high that, even at the highest explored temperatures the structural relaxation is still out of the spectral window.

A more careful inspection of the light scattering data, however, shows that they present a somewhat singular behavior. In fact, the ν_l data experience a strikingly broad relaxation region that essentially covers the whole explored temperature range, including the temperature region in the glassy phase. This behavior strongly suggests the presence of a secondary relaxation process in the GHz frequency range [12,13]. It is our aim to show that a proper Brillouin light scattering line-shape fitting analysis is able to characterize this secondary process, and we will come to this point in the following paragraph. For the moment, we conclude the inspection of the acoustic properties of OTP by checking the correctness of the previously reported normalization of the $S(q,\omega)$ spectra using the following argument, proposed by Pinnow *et al.* [50].

The total integral of the $S(q,\omega)$, via Eq. (11), is proportional to the isothermal compressibility χ_T and can be considered as the sum of three components: (i) a first nonoscillatory contribution due to the isobaric entropy fluctuations, whose area is proportional to $\chi_T - \chi_S$, where χ_S is the adiabatic compressibility; (ii) an oscillatory contribution, which is related to the propagation of the sound waves in the fluid and whose associated spectral integral contributes to χ_S via $\chi_S(\omega_p)$, i.e., the adiabatic compressibility calculated at the frequency ω_p; (iii) a second nonoscillatory contribution, which is related to the active relaxations. Specifically, the oscillatory contribution $2I_B$ to the spectral integral reads

$$2I_B = \rho k_B T \chi_S(\omega_p)/M. \tag{29}$$

Moreover, the area of the oscillatory contribution can be

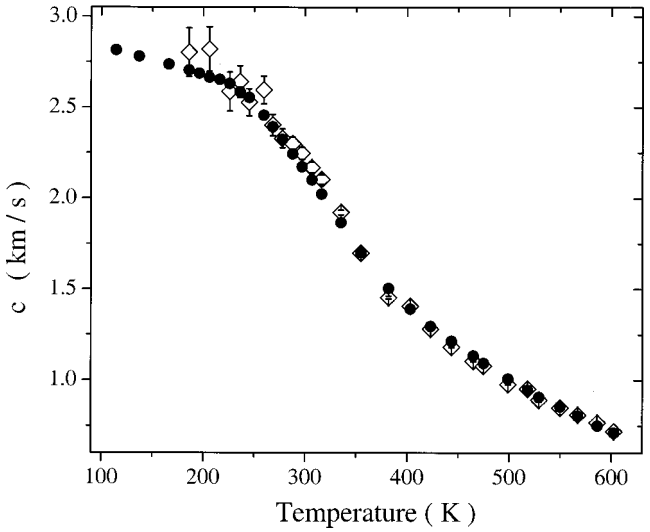

FIG. 8. Sound velocity as a function of temperature determined from integral properties of the $S(q,\omega)$ spectra via Eq. (31) (open diamonds) as compared to the sound velocity obtained from the Brillouin peak positions (full circles). The good agreement between these two independent data sets demonstrates the reliability of the presented normalization procedure for the $S(q,\omega)$ spectra.

also easily measured from the spectra (i) by measuring the area I_+ of the Brillouin peak in the frequency range $\omega > \omega_p$, and (ii) by determining the total integral oscillatory contribution $2I_B$ via the relation [50]

$$I_B \approx 2I_+\left(1+\frac{\Gamma_p}{\omega_p}\right). \tag{30}$$

In fact, at frequencies higher than ω_p the Brillouin resonance ''cuts'' the integral contribution of the active relaxations and only leaves the oscillatory contribution. Moreover, the term in parentheses on the rhs of Eq. (30) takes into account the intrinsic asymmetry of the Brillouin lines and is added in order to achieve a high accuracy ($\pm 2\%$) in obtaining I_B [50]. Equations (29) and (30) have been used to determine, starting from the absolute integral values of I_+ calculated from the spectra presented in Fig. 5, the sound velocity through the simple relation

$$c(\omega_p) \approx \sqrt{\frac{k_B T/M}{4I_+(1+\Gamma_p/\omega_p)}}. \tag{31}$$

The results of this calculation are presented in Fig. 8 (open diamonds) and are compared to the velocity data obtained from Table I (full circles). It is worth noting that the present derivation of $c(\omega_p)$ relies on the knowledge of the absolute value of $S(q,\omega)$. No factor has been used to superimpose the two data sets that indeed are in good agreement. Only at the lowest temperatures the comparison is less satisfactory; in that range, in fact, the Brillouin peaks are narrow and the error involved in the integral calculation of I_+ is larger. However, Fig. 8 is a strong support of the reliability of the normalization procedure based on the calculation of the second moments that we have introduced in the preceding section.

B. Line-shape fitting analysis

A line-shape fitting analysis of the $S(q,\omega)$ spectra reported in Fig. 5 will now be presented and discussed on the basis of Eqs. (14) and (15) together with Eqs. (17) and (20). In order to extract a reliable information from this analysis, a minimal number of free-fitting parameters has to be considered.

For what concerns the thermal diffusion term, it can be fixed using literature values for γ and D_T. In fact, γ can be derived from the relation: $\gamma=[1-T\alpha_P^2(\rho c_P \chi_T)^{-1}]^{-1}$, where data for the mass density ρ, the isothermal compressibility χ_T, and the isobaric expansion coefficient α_P are available from Ref. [48], and data for the constant-pressure specific heat c_P are available from Ref. [51]. Starting from these data, the constant values $\gamma^g=1.06$ in the glassy phase and $\gamma^l=1.20$ in the liquid phase are used in the following. Moreover, $D_T=k\gamma/(\rho c_p)$ can be determined from the additional knowledge of the thermal conducibility data available from Ref. [46,47,52]. Starting from these data, the constant values $D_T^g=1.4\times10^{-3}$ cm^2 s^{-1} in the glassy phase and $D_T^l=0.6\times10^{-3}$ cm^2 s^{-1} in the liquid phase are used in what follows. It has to be underlined that the explicit introduction of the thermal diffusion process into the memory function Eq. (15) has more a formal than a practical justification for the sake of the line-shape data analysis to be described in what follows. In fact, the diffusion process essentially contributes to the isotropic spectrum through a Lorentzian centered at $\nu=0$ and with a FWHM which, given the previous numbers, amounts to ≈ 0.07 GHz. However, since our experimental spectra only start at ≈ 0.4 GHz, they are really only marginally affected by the thermal diffusion process. The only relevant role of this process, as a matter of fact, is to keep adiabatic the decay of the density-density correlation function, and thus to renormalize the sound velocity from c_T, the isothermal value that enters Eq. (14), to c_0, the adiabatic value.

The adiabatic sound velocity can also be fixed using literature data. In particular, ultrasonic c_0 measurements for OTP are available in the 300–520 K temperature range [16,17], and can be well represented by the cubic expression

$$c_0 = 3.43\times10^3 - 9.10T + 1.16\times10^{-2}T^2 - 6.63\times10^{-6}T^3, \tag{32}$$

with T in K and c_0 in m/s. Equation (32) has been extrapolated in the whole temperature range (in the liquid phase) covered by the light scattering measurements, namely, from T_g to 600 K, and the corresponding data are reported in Fig. 6 (dotted line). It has to be underlined that the temperature dependence of the ultrasonically measured c_0 in OTP given by Eq. (32) is far from being linear, the latter situation being found in most of the studied glass formers [37]. This somehow atypical behavior has been recently connected to the existence of a sub-MHz relaxation process in OTP [17].

TABLE II. Parameters of the *global* line-shape fitting analysis of the spectra collected in the glassy phase at the temperatures reported in column 1. Columns 2 and 3 report $c_{\infty\alpha}$ and c_∞, respectively. Column 4 reports the ''instantaneous'' viscosity contribution γ_0, fitted as a global parameter on all the spectra. Column 5 reports the characteristic time, τ_f, of the fast relaxation process. Column 6, eventually, reports the final χ^2 value.

T (K)	$c_{\infty\alpha}$ (km/s)	c_∞ (km/s)	γ_0 (10^{-4} cm^2 s^{-1})	τ_f (10^{-12} s)	χ^2
185.9	2.68	2.71	52	33	2.1
206.0	2.63	2.67	52	27	2.1
226.0	2.59	2.64	52	25	2.1
236.2	2.54	2.59	52	25	2.1
245.2	2.51	2.56	52	24	2.1

It has to be underlined, finally, that no free parameter is needed to account for the overall intensity of the spectra, since they have already been put on an absolute scale. However, the considered model has still too many free-fitting parameters in order to reliably fit the spectra reported in Fig. 5, and to additionally reduce this number, additional considerations have to be put in place.

1. Glass

We start from the spectra taken in the glassy phase, closely following an analysis that has already been presented [13]. In this temperature range, the α relaxation is completely frozen ($\omega_p\tau_\alpha \gg 1$), and consequently its contribution to Eq. (17) simply reduces to $K^{CD}_{l,\infty}(\omega)=q^2\Delta^2_\alpha(i\omega\rho)^{-1}$, which corresponds to renormalize the relaxed limit ω_0^2 in Eqs. (14) and (15) to the unrelaxed limit $\omega^2_{\infty\alpha}=\omega_0^2+\Delta^2_\alpha q^2\rho^{-1}$. Consequently, in this temperature range we can use the model based on Eqs. (14), (15), and (17) with only four free-fitting parameters, namely, γ_0, $\omega^2_{\infty\alpha}$, τ_f, and Δ^2_f. This kind of analysis essentially coincides with that reported in Ref. [13], with the only difference that the parameter τ_f introduced in Eq. (17) corresponds to the relaxation time for the memory function itself, and not for the acoustic compliance as previously done [13]. One of the results of that analysis was that the parameter γ_0 comes out to be temperature independent in the $\approx$60-K-wide temperature range below T_g where full $S(q,\omega)$ spectra have been measured. This point is additionally exploited here, where the spectra taken in the glassy phase have been *globally* fitted by minimizing the sum of the usually defined χ^2 functions for the single spectra. Here, γ_0 is a global parameter, i.e., it is constrained to have the same value for all the considered spectra, while the other parameters are kept local. The final parameters of this routine are reported in Table II in terms of $c_{\infty\alpha}$, c_∞, γ_0, and τ_f, together with the final χ^2 value. The quality of the resulting fits is very good, as shown by the example reported in Fig. 9. The results of this analysis are reported in Fig. 6 for what concerns c_∞ (crossed diamonds), in Fig. 10 for τ_f (full squares), and in Fig. 11 for Δ^2_f (full squares).

While the spectra of glassy OTP directly indicate, in a model-independent way, the existence of a relaxational process in the gigahertz frequency range through the presence of a Mountain-like tail at frequencies below the Brillouin peak [13], the present analysis gives us important details on such a process according to the model Eq. (17) that we have used. In particular, the fast relaxation, which we have here described in terms of a simple Debye process, comes out to have a characteristic time on the 10^{-11} s time scale (Fig. 10), and a small strength, as shown both by the difference between the $c_{\infty\alpha}$ and c_∞ data reported in Table II and, directly, by Fig. 11. However, though its strength is small, the fast process gives rise to an important contribution to the Brillouin linewidth just because it is located *exactly* in the Brillouin spectral window. Moreover, the present analysis confirms the quantitative agreement of the γ_0 value obtained with Brillouin light scattering (5.2×10^{-3} cm^2 s^{-1}) with the corresponding value obtained with Brillouin x-ray scattering at much higher q values ($5\pm1\times10^{-3}$ cm^2 s^{-1} [13]) in the considered temperature range. This result suggests that the microscopic contribution added to the memory function has an almost q^2 dependence in a two-decades-wide q range.

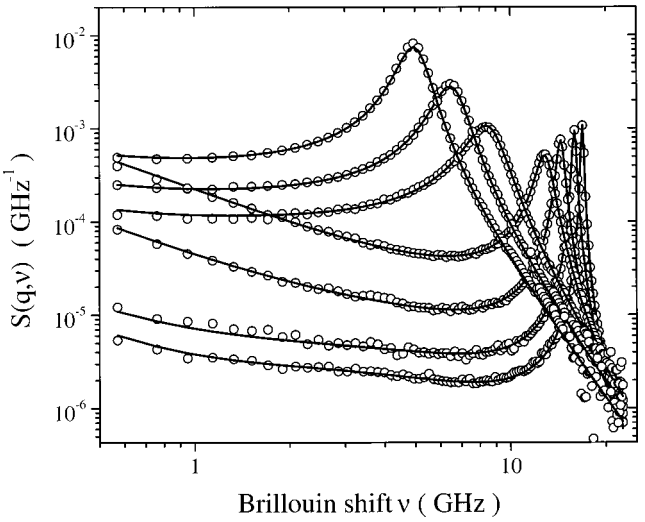

FIG. 9. Comparison of selected $S(q,\omega)$ spectra (open circles) with their corresponding fits (full lines). The spectra refer to the following temperatures (Brillouin peaks from right to left): 236.2, 259.5, 287.9, 316.3, 403.0, 474.8, 549.9. Only $\approx$25% of the data points are shown, for clarity.

2. Supercooled liquid

When one crosses T_g and gets into the supercooled phase, one has to account both for the structural relaxation and for the fast process observed in the glassy phase. Consequently, the full model Eq. (17) has to be used, and one faces the problem of minimizing the number of free parameters. To this extent, γ_0 will be assumed to be temperature independent in the whole temperature range covered here, and will be fixed to the value determined in the glassy phase and reported in Table II. However, this is a noncritical assumption since, as soon as the structural relaxation comes into play, the effect of γ_0 becomes completely negligible. Moreover, we will constraint the structural relaxation by imposing the two following conditions: (i) that its relaxation time is

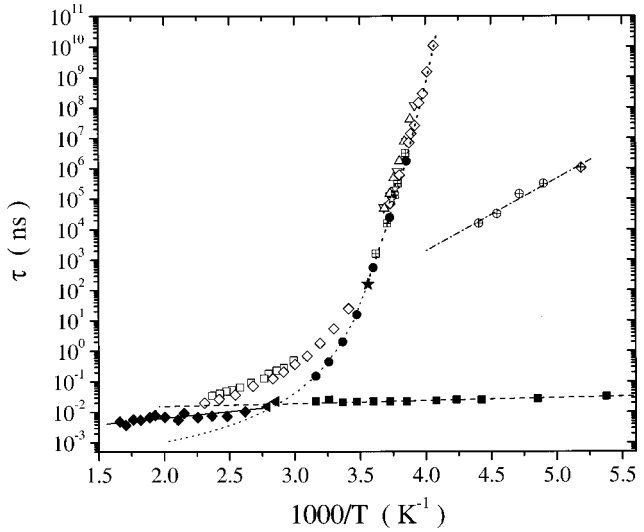

FIG. 10. Activation plot of orthoterphenyl. The results of the lineshape fitting analysis presented here are represented by full symbols: squares for the fast, activated relaxation time; circles for the structural relaxation time, which has been imposed the temperature dependence of the shear viscosity (dotted line); and diamonds for the characteristic times of the average relaxation in the normal liquid phase, which come out to be intermediate between the extrapolation of the structural relaxation and the fast relaxation times. Further values of the average relaxation time have been obtained from the position of the maxima of the apparent longitudinal kinematic viscosity data reported in Fig. 7, and refer to the light scattering (full triangles) and ultrasonic (full star) data. Other literature data are also reported for comparison as open symbols: (i) depolarized light scattering data: squares [20], diamonds [63], up triangles [18] and down triangles [19], the latter ones having been checked to be equal to the characteristic times affecting the isotropic spectra obtained with the photon correlation technique; (ii) dielectric data for the structural relaxation: crossed squares [64] and open stars [65]; (iii) dielectric data for the Johari-Goldstein β relaxation: crossed circles [64] and crossed diamond [66]. The dotted-dashed (dashed, full) line is an Arrhenius fit to the Johari-Goldstein β relaxation (fast relaxation, average relaxation in the liquid phase) data.

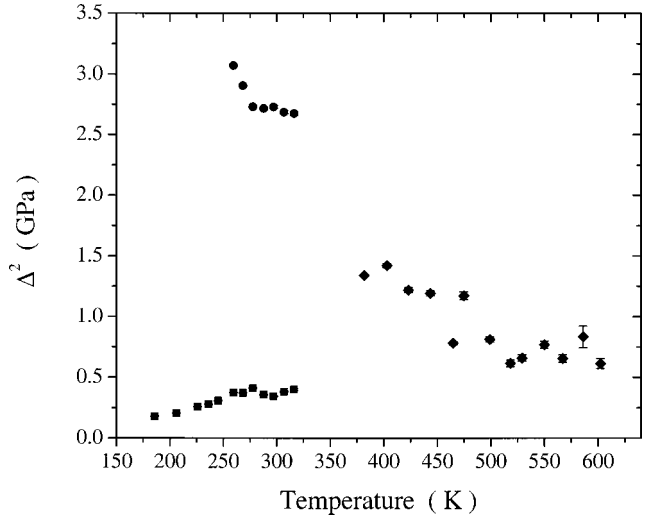

FIG. 11. Temperature dependence of the strength of the relaxation processes introduced in the line-shape fitting analysis presented here. Squares refer to the fast relaxation, and are obtained with two different fitting procedures in the glassy and in the supercooled region. Circles refer to the structural relaxation. Diamonds in the normal liquid phase, finally, refer to the unique average Debye process that has been used to describe the spectra in this temperature range.

essentially proportional to the shear viscosity η_s, i.e., that $\tau_\alpha = J\eta_s$, where J is a constant coefficient with the dimensions of a compliance; and (ii) that the time-temperature superposition principle holds, at least in a restricted temperature range in the supercooled phase, i.e., that the stretching β_{CD} coefficient is temperature independent. With the previous assumptions, a *global* fitting analysis is performed with Δ_α^2, Δ_f^2, and τ_f as *local* parameters and J and β_{CD} as *global* parameters. For what concerns η_s, several data sets are available in the literature [44,46,47,53–57], and they can be reasonably well represented by the Vogel-Fulcher-Tammann law [58,59]:

$$\log_{10}(\eta_s) = A + \frac{B}{T - T_0}, \tag{33}$$

with the following coefficients if one expresses T in K and η_s in P: $A^< = -12.6$, $B^< = 1660$ and $T_0^< = 175$ for $T < 278$ K and $A^> = -3.05$, $B^> = 216$ and $T_0^> = 245.1$ for $T > 278$ K. Moreover, the global fitting analysis is performed according to the following procedure. The first n spectra, in order of increasing temperature, are fitted and the final χ^2 value is compared to that corresponding to the first $n+1$ spectra. For small values of n (and thus for spectra in a limited temperature range above T_g) the final χ^2 value is essentially independent of n, but starting from a certain n^* it shows a definite increase. n^* thus marks the temperature T^* above which the model Eq. (17) becomes unreliable. For the present case, T^* occurs to be close to T_m. Below this temperature, the quality of the fits is very good, as shown both by the examples reported in Fig. 9 and by the final χ^2 value reported in the last column of Table III. In the same table, the complete set of fitting results in this temperature range is reported in terms of $c_{\infty\alpha}$, c_∞, τ_f, $\tau_{\alpha,ave}$, and β_{CD}. Here, $\tau_{\alpha,ave}$ corresponds to the average relaxation time for the considered Cole-Davidson distribution and is given by $\tau_{\alpha,ave} = \tau_\alpha \beta_{CD}$.

The results of the present fitting analysis are reported in Fig. 6 for what concerns c_∞ (crossed diamonds), in Fig. 10 for what concerns τ_f (full squares) and $\tau_{\alpha,ave}$ (full circles), and in Fig. 11 for what concerns Δ_f^2 (full squares) and Δ_α^2 (full circles). One of the interesting points of the fitting procedure that we have just presented is that it is able to give a reliable description of the structural relaxation. In fact, though the temperature dependence of τ_α has been fixed through that of the shear viscosity, an interesting consistency check can be obtained by looking both at the absolute values obtained for $\tau_{\alpha,ave}$, and at the value obtained for the stretching coefficient β_{CD}. The former ones are reported in Fig. 10 (full circles) together with the rescaled shear viscosity curve η_s/J (dotted line). While a general discussion of Fig. 10 will be postponed to the next section, we now compare the $\tau_{\alpha,ave}$

TABLE III. Parameters of the *global* line-shape fitting analysis of the spectra collected in the supercooled phase at the temperatures reported in column 1. Columns 2 and 3 report $c_{\infty\alpha}$ and c_{∞}, respectively. Column 4 reports the characteristic time τ_f of the fast relaxation process. Columns 5 and 6 report *global* parameters: the *average* characteristic time $\tau_{\alpha,ave}$ of the structural relaxation process and the corresponding stretching parameter β_{CD}. Column 7 reports the ratio between the kinematic longitudinal viscosity, obtained as a result of the present analysis, and the kinematic shear viscosity. Column 8, eventually, reports the final χ^2 value.

T (K)	$c_{\infty\alpha}$ (km/s)	c_{∞} (km/s)	τ_f (10^{-12} s)	$\tau_{\alpha,ave}$ (10^{-12} s)	β_{CD}	ν_l/ν_s	χ^2
259.5	2.40	2.47	22	1.7×10^{9}	0.22	4.8	1.1
268.3	2.35	2.42	22	2.5×10^{7}	0.22	4.6	1.1
277.8	2.29	2.37	22	5.6×10^{5}	0.22	4.3	1.1
287.9	2.26	2.33	22	1.6×10^{4}	0.22	4.3	1.1
297.1	2.24	2.31	21	2.0×10^{3}	0.22	4.3	1.1
306.8	2.21	2.29	26	4.5×10^{2}	0.22	4.3	1.1
316.3	2.18	2.27	22	1.5×10^{2}	0.22	4.3	1.1

values obtained here with data obtained for the *same* dynamical variable, the density-density correlation function in the hydrodynamic limit, but using other spectroscopic techniques. In particular, in Fig. 10 the down and up triangle symbols refer to photon correlation spectroscopy data that come out to be very close to each other in both polarized and depolarized scattering configurations [18,19], and thus also correspond to the values for the density-density correlation function; and, additionally, the full star symbol refers to 1 MHz ultrasonic measurements [17], and has been obtained from the maximum of the (apparent) longitudinal viscosity data reported in Fig. 7 since that position marks the condition $\omega\tau=1$. From this comparison in Fig. 10 it comes out clearly that our data are in very good agreement with those obtained from the other two quoted techniques that, operating at a lower frequency, give very reliable τ_α values at temperatures above but close to T_g. A quantitative check on the reliability of our results for the structural relaxation also comes out from the stretching coefficient, which is assumed to be temperature independent in the present analysis, giving a $\beta_{CD}=0.22$ value. In order to compare this value with the one obtained in Ref. [18] with photon correlation spectroscopy, a technique that operates in the time domain, we have to convert the stretching coefficient that we have found into the stretching coefficient β_{WW} of the Williams-Watts stretched exponential function that best represents, in time, the Fourier transform of the Cole-Davidson distribution considered here. Such conversion is readily achieved by means of the relations discussed in detail in Ref. [60], from which we deduce, for our case, a value $\beta_{WW}=0.36$. For a more correct comparison with photon correlation results, which refer to a compliance measurement, this value has additionally to be converted into that of the associated longitudinal compliance, giving $\beta_{WW}=0.43$ [59]. This value agrees well with that found in the quoted photon correlation experiment [18] of $\beta_{WW}\approx 0.5$ around $T=260$ K, though with a slight tendency of increasing when increasing the temperature. For what concerns the structural relaxation strength, reported in Fig. 11, no conclusions on its temperature dependence can be derived due to the limited number of points, though a change of slope around 280 K seems to come out.

Since our description of the structural relaxation has to be considered validated by the positive quantitative comparisons that we have just discussed, it is reasonable to think that also the results that we get for the fast process are reliable. As a matter of fact, the parameters of the fast relaxation that come out from the fitting procedure in the supercooled range are consistent with those obtained in the glassy phase, and show that the fast process is essentially independent of the glass transition. In particular, for what concerns τ_f Fig. 10 shows that it has an almost Arrhenius behavior on a $\approx$150 K temperature range, with a small activation energy $E_a^f=0.28\pm0.08$ kcal/mol; the corresponding Arrhenius fit to the τ_f data is also reported in Fig. 10 (dashed line). For what concerns Δ_f^2, Fig. 11 shows that the fast relaxation strength slightly increases with temperature, though it still remains small as compared to the structural relaxation strength. The parameters of this fast relaxation are the real new information that is obtained with Brillouin spectroscopy, since lower-frequency techniques have no access to it. Further discussion on our results in the supercooled phase will be given in the next section; for the time being, in order to complete our description of the data analysis, we turn to the spectra collected in the normal liquid phase.

3. Normal liquid

By inspecting Fig. 10 we can observe that T^* marks the temperature at which τ_f and $\tau_{\alpha,ave}$ become comparable, and thus marks the temperature at which the twostep relaxation-based model Eq. (17) conceptually begins to fail. Clearly, the temperature region around T^* is difficult to describe since some sort of interference between the two relaxations should be possibly taken into account. This is a quite difficult topic that has been recently discussed [61], but, for the time being, we will leave it aside since it is beyond the aims of the present paper.

As discussed in Sec. II C, at temperatures higher than T^* the most reasonable scenario that we can think of consists in the merging of the α and the fast relaxations in a single process. For this reason, and for the already discussed technical reason that the spectra in the normal liquid phase become less and less informative the higher the temperature, we move to the model Eq. (20) for the analysis of the spectra measured at $T>T^*$. Clearly, this model gives us only an information on the average relaxational dynamics that affects OTP at $T>T^*$, and we will interpret this average dynamics as the dynamics of the expected merged relaxation.

Consistently with what is done in the supercooled phase, also at $T>T^*$ we fix the γ_0 parameter to the value found in the analysis of the spectra collected in the glassy phase. Consequently, the model Eq. (20) presents only two free-fitting parameters, namely the average relaxation time τ and the average strength Δ^2; however, it comes out to be too constrained to fit the spectra. Thus we have to face the problem that, on one side, Eq. (20) appears to be too oversimplified to

TABLE IV. Parameters of the *local* line-shape fitting analysis of the spectra collected in the normal liquid phase at the temperatures reported in Column 1. Column 2 reports c_0, which has been left as a free fitting parameter in the analysis of the spectra at these temperatures. Columns 3 and 4 report c_∞ and the characteristic time τ of the average relaxation process, respectively. Column 5 reports the ratio between the kinematic longitudinal viscosity, obtained as a result of the present analysis, and the kinematic shear viscosity. Column 6, eventually, reports the final χ^2 values.

T (K)	c_0 (km/s)	c_∞ (km/s)	τ (10^{-12} s)	ν_l/ν_s	χ^2
381.7	1.37	1.79	10	4.3	1.8
403.0	1.31	1.78	7.4	5.3	1.1
422.9	1.23	1.66	7.6	6.7	1.0
443.4	1.16	1.61	6.8	7.9	2.2
464.8	1.08	1.41	9.3	9.0	3.8
474.8	1.06	1.54	5.6	9.1	2.2
499.0	0.98	1.36	6.9	9.6	2.4
518.2	0.92	1.24	7.9	9.7	1.3
529.2	0.89	1.24	6.9	9.7	1.9
549.9	0.84	1.26	5.6	10	3.0
567.2	0.80	1.18	5.7	10	2.4
586.2	0.75	1.24	3.8	9.3	3.5
602.3	0.71	1.12	4.9	9.6	4.5

fit our spectra and, on the other side, that our spectra at $T > T^*$ are not informative enough to allow the use of a too complex memory function. In order to solve this problem, and to fit the spectra by adding only one additional parameter, we leave, for $T > T^*$, the relaxed sound velocity c_0 as a free parameter. This in principle is a dangerous choice, since it could completely discredit the model Eq. (20). However, we will show in the following that the results that we get for the fitting parameter c_0 are sufficiently close to the measured ones that we can conclude that Eq. (20), though surely oversimplified, nevertheless, still grasps the main features of the relaxational dynamics. With the present choice of leaving c_0 as a free parameter, we find that, apart from the spectra at $T \approx T^*$, the quality of the fits is again very good, as shown by the examples reported in Fig. 9. In Table IV the complete set of fitting results in this temperature range is reported in terms of c_0, c_∞, and τ, together with the final χ^2 values. The results of this analysis are also reported in Fig. 6 for what concerns c_∞ (crossed diamonds), in Fig. 10 for τ (full diamonds), and in Fig. 11 for Δ^2 (full diamonds).

By inspecting Figs. 10 and 11, we consistently find that in the normal liquid phase of OTP some sort of average, or merged, relaxation process is probed which, for what concerns its strength and relaxation time, has intermediate characteristics between those of the structural and the fast processes. In particular, this average relaxation has an Arrhenius temperature dependence for the characteristic time with an activation energy $E_a^h = 1.3 \pm 0.3$ kcal/mol, which is again intermediate between that of the fast process in the supercooled phase and that corresponding to the structural relaxation (or to the shear viscosity). The corresponding Arrhenius fit to the τ data is also reported in Fig. 10 (full line). Concerning the strength Δ^2, it shows a decreasing trend with increasing temperature, and reduces by $\approx 50\%$ between T_m and T_b. As regards c_0, the results of the fitting routine reported in Table IV can be compared to their expected values given by Eq. (32); while at the highest temperatures the agreement is very good, at lower temperatures the fitted c_0 values appear to overestimate their expected values up to about 6%. This difference, which gives us an idea of the errors involved in the present analysis, has, however, only a marginal effect on the overall picture.

4. Overall considerations

The overall picture summarized by Fig. 10 suggests that T^* is the temperature at which the fast and the structural processes merge in a single channel. This is also confirmed by the two additional data points reported as full triangles in Fig. 10 and obtained from the maxima of the (apparent) longitudinal viscosity (Fig. 7) for the present 180° and the already quoted [21] 90° light scattering experiment; these values, obtained in a completely independent way, fill somehow the gap left from the fitting analysis in the merging region, and show that, for glass formers such as OTP, the $\omega\tau = 1$ condition in Brillouin light scattering spectroscopy falls in a temperature region characterized by strongly entangled relaxation processes.

We now discuss some further checks on the picture coming out from the present analysis and we show that these checks again strongly validate the entire procedure presented here. A first check comes from Eq. (16) which, in connection with the model Eq. (17) gives, for the kinematic longitudinal viscosity: $\nu_l^< = \rho^{-1}(\Delta_\alpha^2 \beta_{CD} \tau_\alpha + \Delta_f^2 \tau_f) + \gamma_0$; and, in connection with the model Eq. (20), gives: $\nu_l^> = \rho^{-1}\Delta^2 \tau + \gamma_0$. The values obtained in this way are reported in Fig. 7 as open stars, and in Tables III and IV in terms of ν_l/ν_s. The ν_l data can be compared, in Fig. 7, with literature ultrasonic data (open up triangles) measured in the 10–50 MHz frequency range [16]. These literature data were checked to correspond to a nondispersive temperature region, and thus directly give the longitudinal kinematic viscosity; moreover, in the small temperature range in which they were measured, they were found to have the same temperature dependence as the shear kinematic viscosity, with a $\nu_l/\nu_s = 4$ ratio, and the quantity $4\nu_s$ is also reported in Fig. 7 (dashed line) and extrapolated to the whole liquid range. From Fig. 7 two conclusions can be drawn. (i) The data for ν_l obtained from the analysis presented here through Eq. (16) compare well with very precise ultrasonic measurements [16]. (ii) At temperatures above $\approx T_m$, the here obtained data for ν_l deviate from the extrapolation of the ultrasonic data, thus meaning that the ratio ν_l/ν_s increases with increasing the temperature. This is actually not at all surprising since it is known that the liquids of the Kneser family, to which OTP most probably belongs [12], are characterized by a ν_l/ν_s ratio increasing with temperature [39]. From a more quantitative point of view, from Table III we can see that, for the ν_l/ν_s ratio in the supercooled range, we get an average value of 4.6 ± 0.3, which corresponds to a $\approx 15\%$ overestimation of the already quoted

value measured with ultrasonics. However, given the frequency range in which our measurement has been obtained, this has to be considered as an excellent quantitative comparison between the two data sets, and moreover it implies that the same precision also applies to the obtained values of $\tau_{\alpha,ave}$.

A further check of consistency comes from comparing the ultrasonic $\nu_l(\omega)$ data measured in the dispersive region at $\nu \approx 1$ MHz [17] (crossed circles in Fig. 7), with the corresponding expectation of model Eq. (17). In the present case, this latter quantity simply corresponds to $\nu_l^{mod}(\omega) = \mathrm{Im}[m(\omega_p)]$, where $m(\omega_p \approx 2\pi \times 1$ MHz) is obtained via Eq. (17) and the final fitting parameters of Table III. The resulting values for ν_l^{mod} are reported in Fig. 7 (full line), and compare again very well with the corresponding experimental data.

A final consistency check is presented in Fig. 6, where the tabulated c_∞ data obtained from the present analysis (crossed diamonds) are compared with the corresponding values (open squares) measured at much higher frequencies with Brillouin x-ray scattering [25]. Once more, the comparison between the outcome of these two different techniques has to be considered, within the experimental uncertainties, very good.

We have thus validated the model used in the lineshape analysis of the spectra reported in Fig. 5, and we have shown that it is able to describe, up to a fairly good approximation, the relaxational dynamics that enters the low-q (hydrodynamic) density-density correlation function in (i) a large range between the megahertz frequency range covered by the ultrasonic technique up to the terahertz frequency range covered by the Brillouin x-ray scattering one; and (ii) in a large temperature range between ≈ 60 K below T_g up to the boiling point. This is our present basis for a more general discussion.

V. DISCUSSION

In the previous section we have quantitatively compared the results of our data analysis with the results obtained using other spectroscopic techniques on the same dynamical variable, namely, the density-density correlation function, and we have now a rather coherent picture of the relaxational dynamics affecting this variable. In order to get a more general understanding of the atomic dynamics in OTP, we now compare the results obtained on the density-density correlation function with those obtained with other correlation functions. The relaxation times of OTP have been measured with most of the available spectroscopic techniques, and consequently a huge amount of data has been collected, and extensive, though necessarily incomplete comparisons have already been reported [62]. Here, we will compare our data for the density-density correlation function only with the results obtained for two of the most commonly investigated correlation functions. Specifically, in Fig. 10 we report the results (i) for the polarizability-polarizability correlation function in the depolarized configuration obtained with photon correlation spectroscopy (open down triangles [19]; open up triangles [18]; open diamonds [22]) and with light scattering measured in the frequency domain (open squares [20]; open diamonds [63]); and (ii) for the electric dipole-dipole correlation function obtained with dielectric spectroscopy and referring both to the structural relaxation (crossed squares [64]; open stars [65]) and to the Johari-Goldstein β-relaxation (crossed circles [64]; crossed diamond, [66]).

Figure 10 clearly shows that in the supercooled phase of OTP one gets very close results for the structural relaxation times that enter the considered three correlation functions. This result is also true for the ^{2}H spin-lattice and the spin-spin relaxation times measured with nuclear magnetic resonance (NMR) spectroscopy [62]. Such a proximity of the structural relaxation times suggests that in this temperature range the different dynamical variables considered here are strongly correlated and directly probe the dynamics of the structural relaxation. This conclusion comes out more explicitely from those studies [65,67] that employ different spectroscopic techniques on the same sample and in the same conditions, in order to avoid possible systematic errors that can heavily bias the comparison of the relaxation times at temperatures close to T_g. In the normal liquid phase, conversely, Fig. 10 shows that the relaxation times corresponding to the density-density correlation function and to the anisotropic polarizability-polarizability one become different, with differences up to one decade in time. In this regime, then, the time-scale proximity induced by the structural relaxation is lost, and different dynamical variables just probe different aspects of the atomic dynamics of a complex molecular liquid.

It has been observed [68] that the anisotropic polarizability-polarizability relaxation time, and more in general both the rotational diffusion correlation time and the translational diffusion coefficient, show a change of regime around the MCT critical temperature, $T_c = 290$ K in OTP [69], where, at least in the ideal version of the theory, the ergodicity breaks down [2]. This observation can be readily appreciated also in Fig. 10, where it can be seen that the anisotropic polarizability-polarizability relaxation time follows the same temperature dependence of the shear viscosity up to about 290 K, and then differentiates from it at higher temperatures. However, the relaxation time of the density-density correlation function seems to have a different behavior: no strong change of dynamics occurs at T_c, the only relevant change taking place around T^*, where the structural and the fast relaxations seem to merge in a single channel. The absence of drastic changes around T_c in the relaxation time of the low-q density-density correlation function is also confirmed by the approximate validity of the time-temperature superposition principle around T_c observed in ultrasonic studies [37]. It would then be interesting to understand whether the low-q density-density correlation function is an exception in showing no relevant change of dynamics at T_c, or, conversely, whether this change only occurs at a correlation-function-dependent temperature, where the considered dynamic variable starts to decouple from the structural relaxation and to probe some kind of specific dynamics.

It has to be reminded that the existence in OTP of a fast relaxation process had already been suggested in the analysis of depolarized-light-scattering spectra [63], though with no

unanimous consensus [70]. In that analysis, two Lorentzian (single time) processes, representing the structural relaxation and a fast one, had been used to fit the spectra, and the fast relaxation characteristic time came out to have essentially the temperature-independent value of $\approx 3\times 10^{-12}$ s [63]. These results are qualitatively in agreement with those that have been presented here, though they refer to a completely different correlation function, and to a different data analysis procedure.

A different discussion has to be reserved for the *coherent* neutron scattering technique, which probes the relaxational dynamics affecting the density-density correlation function at high q, typically at $q>1$ Å. In this kind of studies [69], it has been shown that the relaxational dynamics of OTP in the range $(1-100)\times 10^{-12}$ s can be well analyzed in terms of the β-region of MCT, and thus no sign of an additional fast contribution as presented here has been found. This is an interesting difference between the high-q and the low-q ranges probed by neutron and light scattering, respectively. Clearly, if one trusts both the neutron data analysis [69] and the data analysis presented here, then one has to conclude that the fast relaxation parameters have a strong q dependence, and at high q either the strength goes to zero, or the characteristic time moves out of the neutron scattering time window.

It is also interesting to compare the results that we have obtained here with those obtained by Soltwisch *et al.* in a recent study on the fragile glass former *m*-TCP [11] since both the systems that are studied and the data analyses that are performed are quite similar. Though from a qualitative point of view the results of that study have much in common with those found here (a structural relaxation with a characteristic time proportional to that found by other spectroscopies, in that case NMR; a fast relaxation with a characteristic time, $\tau_f \approx 5\times 10^{-12}$ s, and a very small activation energy, $E_a \approx 0.06$ kcal/mol), there are some relevant differences that deserve to be discussed. In particular, the strength of the fast process is found in Ref. [11] to be essentially zero in the glassy phase and to increase with increasing temperature in the supercooled phase. Consequently, the picture of the fast process that comes out from that study is that of a process strongly related to the glass transition, and the glass transition itself is discussed in terms of a gradual change of fast degrees of freedom into slow ones [11]. This result and the consequent picture is clearly different from the one that comes out from the present analysis, where the fast relaxation is shown to be insensitive to the glass transition and, up to the merging temperature T^*, essentially independent of the structural one. It would be interesting to understand whether this is an intrinsic difference between *m*-TCP and OTP, or whether it is due to the fact that the spectra measured on *m*-TCP did not extend to frequencies low enough and thus did not directly probe the gigahertz relaxational dynamics at temperatures across T_g. Another relevant difference between the two analyses concerns the results for the structural relaxation. In fact, in *m*-TCP it has been found that the structural relaxation time is ≈ 10 times faster than the characteristic times derived from both depolarized and NMR spectra. Conversely, in the present analysis we find that (i) in the supercooled phase the structural relaxation time derived from the fitting analysis is very close to the ones obtained with depolarized, dielectric, and NMR spectroscopy and (ii) in the normal liquid phase the (average) relaxation time strongly depends on the considered dynamical variable. Again, it would be interesting to understand whether this is an intrinsic difference between *m*-TCP and OTP, or whether it is due to the fact that in Ref. [11] the same temperature dependence for the isotropic and depolarized spectra was imposed in the whole temperature range. In fact, our data show that it is also true in OTP that the relaxation time measured from depolarized light scattering and the one obtained from the Brillouin longitudinal viscosity data exploiting the $\omega\tau = 1$ condition are almost one decade apart, see Fig. 10. However, they also show that this does not imply at all that such a strong difference is still there at lower temperatures, in the supercooled range; conversely, the depolarized and the isotropic relaxation times are actually very close to each other in that temperature range.

VI. CONCLUSIONS

High-resolution Brillouin measurements on the fragile glass former orthoterphenyl have been presented, and the dynamic structure factor spectra have been derived. Particular care has been taken in order to obtain spectra covering a large spectral range of approximately two decades and a large temperature range, comprising the whole liquid, both normal and supercooled, range and part of the glassy one. This whole set of spectra has been analyzed using a phenomenological ansatz for the relaxational dynamics.

The data analysis that we have presented in this study suggests the following picture. Two main processes dominate the relaxational dynamics affecting the low-q density-density correlation function of OTP around T_g and in the supercooled liquid phase, namely, the structural and the fast relaxation. They are very different processes: while the former is characterized by a strongly temperature-dependent time scale, the time scale of the latter depends on temperature rather smoothly, with an Arrhenius behavior and a low activation energy $E_a^f = 0.28 \pm 0.08$ kcal/mol; while the former has a large strength, which seems to decrease with increasing temperature, the latter has a smaller strength which, conversely, increases with increasing temperature; more importantly, while the former strongly depends on the glass transition, practically diverging close to T_g, the latter seems to be almost insensitive to it, and survives unchanged in the glassy phase. At one point, which in OTP occurs to be close to the melting point T_m, these two relaxations have comparable time scales, and at even higher temperatures they appear to merge in a single relaxation process with intermediate values of strength and relaxation time. This average process is characterized by a strength that decreases with increasing temperature, and by an activation energy of $E_a^h = 1.3 \pm 0.3$ kcal/mol, to the point that at the boiling point its characteristic time is still somehow longer than 1×10^{-12} s.

Beside these two relaxations, a further microscopic process, modeled in terms of a Markovian, instantaneous relaxation, is here considered and related to the acoustic absorp-

tion measured at high wave numbers [13]. Its temperature dependence comes out to be negligible in the range considered here, and in particular in the $\approx$60-K range below T_g where the line-shape analysis of the Brillouin spectra has been presented. No extrapolations are allowed from the present analysis to lower temperatures in view of the occurrence in different systems of relaxation phenomena in the light scattering Brillouin spectra at low temperatures [40]. In order to describe the Brillouin spectra down to those low temperatures, consequently, a more refined model than that presented here has to be used.

The picture of the relaxational dynamics that we have presented here is consistent with the other literature data on the low-q density-density correlation function of OTP, and in particular with ultrasonics [16,17] and photon correlation spectroscopy [18,19] data. The comparison with the results obtained on other correlation functions shows additionally the following points. (i) The structural relaxation in the supercooled regime affects all the correlation functions in a very similar way. (ii) In the same temperature range where the structural relaxation shows this time-scale proximity, our analysis shows a reasonable consistency with the time-temperature superposition principle. (iii) The relaxation time of the low-q density-density correlation function shows no relevant change of dynamics at T_c, contrary to what has been found on other correlation functions [68]. The only relevant temperature seems to be $T^* \approx T_m$, where the structural and the fast processes seem to merge into a single channel. (iv) At temperatures higher than T^*, different correlation functions measure different relaxation times, as one would in principle expect in a polyatomic, complex liquid like OTP.

We associate the fast process that emerges from this analysis to a coupling among the translational and one or more (still unidentified) intramolecular degrees of freedom [30], i.e., to a vibrational relaxation. The main motivations for this attribution come from the following points. (i) The fast process is insensitive to the glass transition, as it shows very similar characteristics, both relaxation time and strength, on both sides of T_g. (ii) A very similar fast process is also present in the single-crystal phase of OTP [24], thus being completely independent on the intermolecular packing. (iii) The fast process only affects the longitudinal dynamics and not the transverse one, which is consistent with the fact that, in first approximation, a vibrational relaxation does not affect the transverse dynamics [24]. This interpretation of the fast process is consistent with the results obtained mainly by ultrasonics in many organic liquids [39].

It is interesting to note that coherent neutron scattering experiments, which measure the high-q density-density correlation function, do not probe the fast process [69]. The fast process then seems to become less and less relevant as one increases q, and seems to be a peculiarity of the low-q density-density correlation function. At low q it probably superimposes on the MCT β region, thus making it difficult to use the Brillouin light scattering spectra of systems similar to OTP to check the theory itself.

[1] See, for example, *Rheology*, edited by F.R. Eirich (Academic Press, London, 1958–1970), Vols. 1–5.

[2] W. Götze, in *Liquids, Freezing and the Glass Transition*, edited by J.P. Hansen, D. Levesque, and J. Zinn-Justin (North-Holland, Amsterdam, 1991), pp. 289–503.

[3] R. Schilling and T. Scheidsteger, Phys. Rev. E **56**, 2932 (1997); S. Kämmerer, W. Kob, and R. Schilling, *ibid.* **56**, 5450 (1997); T. Franosch, M. Fuchs, W. Götze, M.R. Mayr, and A.P. Singh, *ibid.* **56**, 5659 (1997).

[4] For a recent review, see: W. Götze, J. Phys.: Condens. Matter **11**, A1 (1999).

[5] G. Li, W.M. Du, J. Hernandez, and H.Z. Cummins, Phys. Rev. E **48**, 1192 (1993).

[6] S. Loheider, G. Vögler, I. Petscherizin, M. Soltwisch, and D. Quitmann, J. Chem. Phys. **93**, 5436 (1990).

[7] W.M. Du, G. Li, H.Z. Cummins, M. Fuchs, J. Toulouse, and L.A. Knauss, Phys. Rev. E **49**, 2192 (1994).

[8] D. Fioretto, L. Palmieri, G. Socino, and L. Verdini, Phys. Rev. B **50**, 605 (1994).

[9] S.N. Yannopoulos, G.N. Papatheodorou, and G. Fytas, Phys. Rev. E **53**, R1328 (1996); Phys. Rev. B **60**, 15 131 (1999).

[10] A. Aouadi, M.J. Lebon, C. Dreyfus, B. Strube, W. Steffen, A. Patkowski, and R.M. Pick, J. Phys.: Condens. Matter **9**, 3803 (1997).

[11] M. Soltwisch, G. Ruocco, B. Balschun, J. Bosse, V. Mazzacurati, and D. Quitmann, Phys. Rev. E **57**, 720 (1998).

[12] G. Monaco, L. Comez, and D. Fioretto, Philos. Mag. B **77**, 463 (1998).

[13] G. Monaco, D. Fioretto, C. Masciovecchio, G. Ruocco, and F. Sette, Phys. Rev. Lett. **82**, 1776 (1999).

[14] D. Fioretto, L. Comez, G. Socino, L. Verdini, S. Corezzi, and P.A. Rolla, Phys. Rev. E **59**, 1899 (1999).

[15] A. Aouadi, C. Dreyfus, M. Massot, R.M. Pick, T. Berger, W. Steffen, A. Patkowski, and C. Alba-Simionesco, J. Chem. Phys. **112**, 9860 (2000).

[16] G. D'Arrigo, J. Chem. Phys. **63**, 61 (1975).

[17] G. Monaco, B. Balschun, D. Fioretto, G. Ruocco, and M. Soltwisch (unpublished).

[18] G. Fytas, C.H. Wang, D. Lilge, and Th. Dorfmüller, J. Chem. Phys. **75**, 4247 (1981).

[19] G. Fytas, Th. Dorfmüller, and C.H. Wang, J. Phys. Chem. **87**, 5041 (1983).

[20] Y. Higashigaki and C.H. Wang, J. Chem. Phys. **74**, 3175 (1981).

[21] C.H. Wang, X.R. Zhu, and J.C. Shen, Mol. Phys. **62**, 749 (1987).

[22] E.W. Fischer, Ch. Becker, J.-U. Hagenah, and G. Meier, Prog. Colloid Polym. Sci. **80**, 198 (1989).

[23] F. Nizzoli and J.R. Sandercock, in *Dynamical Properties of Solids*, edited by G. Horton and A.A. Maradudin (North-Holland, Amsterdam, 1990).

[24] G. Monaco, S. Caponi, R. Di Leonardo, D. Fioretto, and G. Ruocco, Phys. Rev. E **62**, R7595 (2000).

[25] C. Masciovecchio, G. Monaco, G. Ruocco, F. Sette, A. Cunsolo, M. Krisch, A. Mermet, M. Soltwisch, and R. Verbeni,

Phys. Rev. Lett. **80**, 544 (1998); G. Monaco, C. Masciovecchio, G. Ruocco, and F. Sette, *ibid.* **80**, 544 (1998).
[26] R. Loudon, *The Quantum Theory of Light* (Clarendon Press, Oxford, 1973).
[27] J.P. Boon and S. Yip, *Molecular Hydrodynamics* (Dover Publications, New York, 1991).
[28] U. Balucani and M. Zoppi, *Dynamics of the Liquid State* (Clarendon Press, Oxford, 1994).
[29] V. Mazzacurati and G. Ruocco, Mol. Phys. **61**, 1391 (1987).
[30] S. Mossa (private communication). Work is in progress on a molecular dynamics simulation of OTP that includes internal vibrations in order to identify the macroscopic origin of the fast relaxational dynamics discussed in Ref. [24] and in the present paper.
[31] C.H. Wang, *Spectroscopy of Condensed Media* (Academic Press, New York, 1985).
[32] G.B. Benedek and K. Fritsch, Phys. Rev. **149**, 647 (1966).
[33] A. Latz and M. Letz, Eur. Phys. J. B **19**, 323 (2001).
[34] G. Monaco *et al.* (unpublished).
[35] R. Zwanzig, in *Lectures in Theoretical Physics*, edited by W. Brittin (Wiley-Interscience, New York, 1961), Vol. 3, pp. 106–141; H. Mori, Prog. Theor. Phys. **33**, 423 (1965).
[36] C. Dreyfus, A. Aouadi, R.M. Pick, T. Berger, A. Patkowski, and W. Steffen, Eur. Phys. J. B **9**, 401 (1999).
[37] G. Harrison, *The Dynamic Properties of Supercooled Liquids* (Academic Press, New York, 1976).
[38] D.V. Davidson and R.H. Cole, J. Chem. Phys. **19**, 1484 (1951).
[39] K.F. Herzfeld and T.A. Litovitz, *Absorption and Dispersion of Ultrasonic Waves* (Academic Press, London, 1965).
[40] See, for example, R. Vacher and J. Pelous, J. Chim. Phys. Phys.-Chim. Biol. **82**, 311 (1985).
[41] V. Mazzacurati, P. Benassi, and G. Ruocco, J. Phys. E **21**, 798 (1988).
[42] R.D. Mountain, Rev. Mod. Phys. **38**, 205 (1966); R.D. Mountain, J. Res. Natl. Bur. Stand., Sect. A **70A**, 207 (1966).
[43] C.J. Montrose, V.A. Solovyev, and T.A. Litovitz, J. Acoust. Soc. Am. **43**, 117 (1967).
[44] J.N. Andrews and A.R. Ubbelohde, Proc. Phys. Soc., London, Sect. A **228**, 435 (1955).
[45] R.J. Greet and D. Turnbull, J. Chem. Phys. **46**, 1243 (1967).
[46] G. Friz, G. Kuhlbörsch, R. Nehren, and F. Reiter, Atomkernenergie **13**, 25 (1968), and references therein.
[47] W.H. Hedley, M.V. Milnes, and W.H. Yanko, J. Chem. Eng. Data **15**, 122 (1970), and references therein.
[48] M. Naoki and S. Koeda, J. Phys. Chem. **93**, 948 (1989).
[49] A. Patkowski, W. Steffen, H. Nilgens, E.W. Fischer, and R. Pecora, J. Chem. Phys. **106**, 8401 (1997).
[50] D.A. Pinnow, S.J. Candau, J.T. LaMacchia, and T.A. Litovitz, J. Acoust. Soc. Am. **43**, 131 (1967).
[51] S.S. Chang and A.B. Bestul, J. Chem. Phys. **56**, 503 (1972).
[52] P.K. Dixon and S.R. Nagel, Phys. Rev. Lett. **61**, 341 (1988).
[53] E. McLaughlin and A.R. Ubbelohde, Trans. Faraday Soc. **54**, 1804 (1958).
[54] R.J. Greet and D. Turnbull, J. Chem. Phys. **47**, 2185 (1967).
[55] W.T. Laughlin and D.R. Uhlmann, J. Phys. Chem. **76**, 2317 (1972).
[56] M. Cukierman, J.W. Lane, and D.R. Uhlmann, J. Chem. Phys. **59**, 3639 (1973).
[57] W. Steffen (private communication).
[58] C. Hansen, F. Stickel, T. Berger, R. Richert, and E.W. Fischer, J. Chem. Phys. **107**, 1086 (1997), and references therein.
[59] G. Monaco, Ph.D. thesis, University of L'Aquila, Italy, 1997.
[60] C.P. Lindsey and G.D. Patterson, J. Chem. Phys. **73**, 3348 (1980).
[61] A. Arbe, D. Richter, J. Colmenero, and B. Farago, Phys. Rev. E **54**, 3853 (1996).
[62] See, for example, Fig. 3 in: E. Rössler and W. Schnauss, Chem. Phys. Lett. **170**, 315 (1990).
[63] W. Steffen, A. Patkowski, G. Meier, and E.W. Fischer, J. Chem. Phys. **96**, 4171 (1992).
[64] G.P. Johari and M. Goldstein, J. Chem. Phys. **53**, 2372 (1970).
[65] M.S. Beevers, J. Crossley, G.C. Garrington, and G. Williams, J. Chem. Soc., Faraday Trans. 2 **73**, 458 (1977).
[66] M. Naoki and M. Ueda, J. Chem. Phys. **90**, 1169 (1989).
[67] L. Wu, P.K. Dixon, S.R. Nagel, B.D. Williams, and J.P. Carini, J. Non-Cryst. Solids **131-133**, 32 (1991).
[68] E. Rössler, Phys. Rev. Lett. **65**, 1595 (1990).
[69] W. Petry, E. Bartsch, F. Fujara, M. Kiebel, H. Sillescu, and B. Farago, Z. Phys. B: Condens. Matter **83**, 175 (1991); E. Bartsch, F. Fujara, J.F. Legrand, W. Petry, H. Sillescu, and J. Wuttke, Phys. Rev. E **52**, 738 (1995); A. Tölle, H. Schober, J. Wuttke, and F. Fujara, *ibid.* **56**, 809 (1997).
[70] H.Z. Cummins, Y.H. Hwang, G. Li, W.M. Du, W. Losert, and G.Q. Shen, J. Non-Cryst. Solids **235-237**, 254 (1998); A. Patkowski, W. Steffen, and E.W. Fischer, *ibid.* **235-237**, 268 (1998).